Chapter 7

Observation of the Load Torque of an Electrical Machine

7.1. Introduction

The requirements on speed and position control for electro-mechanical actuators have a strong impact on the control loops of variable speed drives. The electromagnetic torque must be perfectly controlled to obtain the most satisfying evolutions in speed or position. Regardless of the care we take in the construction of the electrical machine and the power quality of this machine, the resulting electromagnetic torque very often contains a ripple. It is increased in so far as electromotive forces are not sinusoidal and/or the relation between decoupling frequency and fundamental frequency is too low. This torque ripple is visible in the speed and position behavior of the machine, notably at low speed.

In addition, the resulting mechanical loads often have undefined characteristics in terms of the low-speed neighborhood or even zero or quasi-zero speeds. The variable speed drive's control in these specific operation zones can turn out to be problematic and its traditional control laws are often wrong. The study proposed in this chapter contributes to this theme, by developing a solution for the improvement of the global actuator behavior.

The major solution considered is based on the association of a powerful control method based on speed and position state feedback presumed measurable here and a method of reconstruction of the total load torque. The main contribution involves the

---

Chapter written by Maurice FADEL and Bernard DE FORNEL.

Electrical Actuators: Identification and Observation Edited by Bernard de Fornel and Jean-Paul Louis

torque observer that can observe effort disruptions because of its structure and operation. They are inherent to the internal structure of the electrical machine used (cogging torque, electromotive force distortion, etc.) and also come from exogenous parametric modifications relative to the resulting load. In this way, the observer provides information representing the series of disruptions experienced by the axis of rotation independently of the nature of these modifications and original cause. This quantity representing the torque to be compensated is then injected in the control law in order to smooth the machine's effective torque. The set thus functions in disturbance rejection.

The solutions presented here are based on studies conducted at Laboratoire d'Electrotechnique et d'Electronique Industrielle de Toulouse (LEEI), resulting in experimental prototypes digitally powered and run. Several results, most of them experimental, confirm the relevant character of the robustness approach and qualities in relation to the parameter variations of the load and/or machine. The choice of the observer's dynamic compared with the setup process and the number of sensors used is being carefully examined.

7.2. Characterization of a load torque relative to an axis of rotation

7.2.1. *Introduction*

The drive of a mechanical load in rotation with the help of an electrical machine is often the basis of disruptions linked to the specific characteristics of the useful load (pump, cooling fan, etc.) as well as the internal characteristics of the motor (roll and bearing quality, etc.). Even if the powered load has a specific and known behavior in relation to speed, the appearance of an external event can lead to significant modifications of the effort required by the motor and result in undesirable behavior. In addition, seen as a torque generator, the electrical motor usually reveals some structural imperfections that can compromise the quality of the drive. The internal efforts experienced by this axis can be separated into two categories based on whether they depend on the nature of the contact between the fixed and mobile parts (friction, etc.) or whether they depend on the remote interaction between these two same parts (aerodynamic efforts, magnetic interactions, etc.). Globally, the load relating to an axis in rotation is complex and its characteristics depend on many factors, particularly speed of rotation, amplitude, and signal. In the following, we illustrate these specific efforts by characterizing them according to speed and in the context of variable speed drive type operations.

In real systems, load torques are very different depending on whether we are dealing with a cooling fan, a pump, a piston machine, a hoisting system, or a

machining process, etc. We consider the main components of the load torque and internal friction torque encountered in major applications.

7.2.2. *Disruptions of the electrical machine torque*

7.2.2.1. *Generation of the electromagnetic torque*

Within the synchronous machine, the interaction between a magnetic field and an electrical current is at the basis of the production of an electromagnetic torque. Its quality is linked to the purity of the three-phase current system imposed to the stator as well as the actual structural characteristics, notably magnetic. Among the causes that can trigger a change in the torque produced, we note:

– the imposition of currents that are not perfectly sinusoidal: by a residual ripple inherent to limited decoupling frequency power, or by a slight imbalance between the phases;

– determination of electromotive forces, which are not perfectly sinusoidal, linked to a specific geometry of the stator, or the more rare existence of a certain saturation of the magnetic circuit.

Generally, the existence of current harmonics (hi) or electromotive force harmonics (he) is at the basis of torque harmonics obtained by the combination corresponding to Table 7.1.

		Current harmonics						
EMF harmonics	he \ hi	1	5	7	11	13	17	19
	1	0	6	6	12	12	18	18
	5	6	0	12	6	18	12	24
	7	6	12	0	18	6	24	12
	11	12	6	18	0	24	6	30
	13	12	18	6	24	0	30	6
	17	18	12	24	6	30	0	36
	19	18	24	12	30	6	36	0

Table 7.1. *Major torque harmonics generated by current and electromagnetic force harmonics*

In this way, emerging torque harmonics are of order 6, 12, 24, etc., that is, multiplied by six times the powering frequency of the machine. We should note that by action on the control, it is possible to act on injected current harmonics and thus offset torque distortion caused by an electromotive force harmonic by generating a corresponding current harmonic. For example, an order five harmonic on current can block an order six torque ripple triggered by an electromotive force having an order seven harmonic. This methodology goes beyond the scope of this book, and for more information, we can refer to reference [GAS 04].

If the resulting electromagnetic torque is constant in terms of accepted tolerance, the cogging torque can trigger ripples and modify the quality of the generated force.

7.2.2.2. *The cogging torque*

The cogging torque is the result of the interaction between rotor windings or the magnet and magnetic circuit constituted by the rotor and the stator. The presence of slots and the resulting reluctance variation are responsible for this effect. This is translated by preferential rotor positions compared to the stator. This effect is very disruptive in the case of induction machine position control and can be seen without power for a magnet machine and in the presence of excitation for a wound induction machine. In any case, the disruptive torque remains independent from the stator current. This torque, also called slot torque, depends on the constitution of the machine's magnetic circuit, and more specifically, the number of slots [MTS 93]. These slots receive motor windings and are equally distributed on the stator and rotor; they create air-gap variations when the rotor moves in relation to the stator. When the rotor is powered, it naturally moves into a position that minimizes circuit reluctance, as viewed by the rotating field. This minimization of reluctance corresponds to the minimization of the global air gap viewed by the field winding. When the rotor is in a stable angle position and an external action moves it away, this torque tends to bring it back to this position. If the rotor is in an unstable position (Figure 7.1) and an external action moves it away, this torque brings it back to the next stable attitude angle.

If Ne represents the number of slots in the stator and Pp the number of pole pairs, the number of periods in a mechanical turn is defined by:

$$\mathrm{Np} = PPCM(\mathrm{Ne}, 2\times \mathrm{Pp}) \qquad [7.1]$$

The resulting cogging torque is expressed by:

$$C_{\mathrm{d}}(\theta) = C_{\mathrm{d1}} \cdot \sin\left(\frac{\mathrm{Ne}}{2\cdot \mathrm{Pp}\cdot \mathrm{Np}}\times\theta\right) + C_{\mathrm{d2}} \cdot \sin\left(2\times\frac{\mathrm{Ne}}{2\cdot \mathrm{Pp}\cdot \mathrm{Np}}\times\theta\right) + \cdots \qquad [7.2]$$

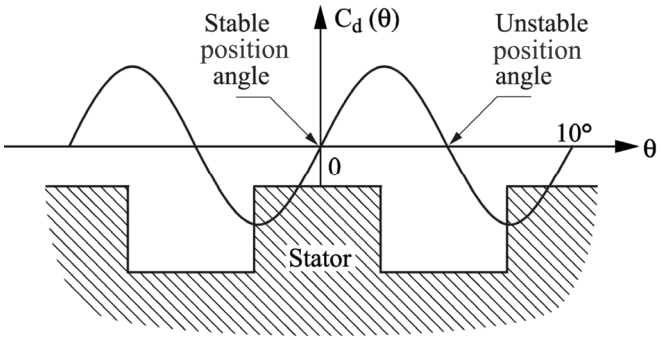

Figure 7.1. *First harmonic of the cogging torque*

The values of C_{di} can be obtained by field calculation as they depend mainly on the geometry of the motor. We can also carry out a low-speed test by controlling the speed to a constant value and by evaluating current distortion. The disruptive effects of this torque can be compensated in different ways:

– using automatic techniques to act on the motor's current control. This control is modulated according to the observation of cogging torque effects on the variable to control [MTS 93, VOR 95];

– compensating this cogging torque by powering the machine with currents where waveshapes are first calculated according to the structure of the powered machine [CLE 95].

In addition, a careful construction including a set of slots or magnets makes it possible to significantly decrease this amplitude of the disruptive torque. In terms of design, the choice of the number of slots can efficiently influence this ripple.

7.2.2.3. *Other disruptive torques non-linked to contact*

The torque produced by an electrical machine can also experience disruptions that are difficult to measure, and which obey to uncertain models. In this regard, we note the existence of an imbalance linked to a compensation fault with moving parts, or an alignment fault of drive axes, not absorbed by coupling. These constraints generate an additional resistant torque disturbing the position as well as the speed operation. In the same vein, aerodynamic reaction forces located in the air gap and linked to rotor movement are at the basis of additional efforts noticeable at high speed notably.

7.2.3. *Load torque disruptions by modification of contact actions*

In a rotation drive, the moving part is in contact with the fixed part through an adapted device, revealing specific characteristics based on the speed of rotation.

7.2.3.1. *Low-speed friction*

We have three types of friction. The first one is called static friction and occurs only when both parts in contact (bearings and axis of rotation) are not moving, consequently at zero speed. The other two types of friction occur when the speed is not zero. They are solid friction or dry friction, independent from speed, and viscous friction, proportional to speed. We note here the problem with simulating these phenomena inherent to the definition of speed around zero.

Viscous friction is the only linear friction; it is, therefore, the only one considered for the determination of linear control algorithms. However, this approach is sometimes insufficient to achieve precise position control. There are other types of friction:

– *Static friction*: This is the force to overcome in order to move a part that is in contact with another part. A minimal torque is necessary to trigger the actuator's rotation. This maximal torque value of static friction (C_0) is sometimes called "break-off torque" or "starting torque". It depends mainly on the contact pressure between both parts and the nature of matters in contact [FÖR 95]. An increase in contact pressure results in an increase in the maximum value of the static friction torque. This contact pressure is created by radial forces occurring in the actuator bearings and load bearings. For hoisting applications, the maximum value of the static friction torque is not previously known because of ignorance about the mass to hoist. The sum of torques applied to the axis (other than the static friction torque) can have an infinite number of values without triggering any rotation, as long as this sum remains lower than the maximum value of the static friction torque, hence, the existence of limited cycles often observed during a mass hoisting test. Because of static friction in bearings, the variation of control dimension has no immediate effect on the actuator. When the sum of torques, other than the static friction torque, exceeds the maximum value of static friction torque, the actuator starts rotating.

– *Dry friction*: The torque corresponding to this friction is independent of speed, but it is defined for a non-zero speed. As with other types of friction, dry friction hinders movement. Its value is given by the Coulomb law and depends on the contact pressure between both parts as with the maximum value of static friction. Its value is generally lower than the maximum static friction value [FÖR 95] and results in this case in a constant resistant torque.

– *Viscous friction*: The viscous friction torque is proportional to speed and hinders movement. The factor of proportionality is generally called "coefficient of friction" and depends on the viscosity of the lubricant used in the bearings [FÖR 95]. It can be the subject of significant variations depending on the ambient temperature. It is also possible to observe a modification of this coefficient by effect of ageing of grease used.

– *Combination of friction types*: The different friction types described here can be represented by a characteristic (Figure 7.2) illustrating friction torque (C_{frot}) according to speed [FÖR 95, JOH 92]. The characteristic is symmetrical, but the different terms making up the friction torque are not necessarily equal in absolute value; they can take different values depending on the rotation direction, and especially on the type of stress from actuator bearings.

The characteristic (Figure 7.2) is close to the Striebeck friction [FÖR 95, LIG 95], hence the following notes:

– Close to zero speed ($\Omega \in [-\Omega_0, \Omega_0]$), a static friction zone appears, different from the one obtained by the model described earlier where this friction exists only at zero speed. The existence of this zone makes the numerical simulation of static friction easier [FÖR 95, JOH 92].

– During the transition between static friction and other types of friction, the "*stiction*" zone corresponds to a quick decrease of the friction torque when the speed increases [GOM 92]. Reciprocally, in slowdown phase, the friction torque quickly increases and can abruptly block the actuator. The actuator is then in static friction mode, which can compensate the gap between the motor torque and load torque and keep the actuator stopped. This gap can come from the control law, which is unable to adapt the motor torque quickly enough to variations of the friction torque because of its dynamic that is too slow. We now consider a simulation of non-linear friction to achieve representations of these types of friction.

7.2.3.2. *Non-linear friction simulation*

The simulation example presented here shows the implementation of non-linear friction models. It integrates specific conditions (cogging torque, quantification, sampling, filtering, etc.). The values retained to simulate non-linear friction are evaluated empirically from different experimental tests.

A block simulating non-linear friction (C_{fnl}) is contained in the simulation diagram (Figure 7.3). According to this diagram, non-linear friction is internal to the actuator and hinders all torque stresses ($\Sigma Cple$), including the cogging torque. The simulation diagram of non-linear friction (Figure 7.4) distinguishes between the static friction mode and the dry friction mode, depending on speed Ω of the actuator (Figure 7.2). If Ω is higher than Ω_0 in absolute value, the actuator is in dry friction

mode, and the corresponding non-linear friction torque (C_{fsec}) is independent of speed. The mechanical equation is then written as:

$$J \cdot \frac{\mathrm{d}\Omega}{\mathrm{d}t} = \Sigma Cple - f \cdot \Omega - \underbrace{C_{\text{fsec}} \cdot \text{sign}(\Omega)}_{\text{Dry friction torque}} \qquad [7.3]$$

If Ω is lower than Ω_0 in absolute value, the actuator is in static friction mode. Then, Ω is zero from the moment it is lower in absolute value to Ω_0 [FÖR 95, JOH 92]. This leads to discontinuity in speed, which changes abruptly from 0 to Ω_0 when the mode changes from static friction to dry friction, or conversely.

Since speed is a state variable, such a discontinuity is not admissible. To avoid this discontinuity, we propose the following modeling:

– when $\Omega = 0$, the static friction torque always hinders other torques ($\Sigma Cple$), as long as their sum is inferior in absolute value to the maximum static friction torque (C_0). Speed is zero and

$$J.\frac{\mathrm{d}\Omega}{\mathrm{d}t} = 0 \qquad [7.4]$$

– when $\left|\Sigma Cple\right| > C_0$, the actuator accelerates, and the mechanical equation is then expressed as:

$$J \cdot \frac{\mathrm{d}\Omega}{\mathrm{d}t} = \Sigma Cple - f \cdot \Omega - \underbrace{C_0 \cdot \text{sign}\left(\Sigma Cple\right)}_{\substack{\text{Maximum static} \\ \text{friction torque}}} \neq 0 \qquad [7.5]$$

Speed then becomes different from zero, and from this moment, the static friction torque hinders the movement, and thus, depends on the sign of speed. The mechanical equation becomes:

$$J \cdot \frac{\mathrm{d}\Omega}{\mathrm{d}t} = \Sigma Cple - f \cdot \Omega - \underbrace{C_0 \cdot \text{sign}\left(\Omega\right)}_{\substack{\text{Maximum static} \\ \text{friction torque}}} \qquad [7.6]$$

In this equation, the maximum static friction torque hinders movement, even if speed is not zero. The maximum static friction torque then acts in the same way as the dry friction, but its value is higher. Speed will then evolve, and when it is higher than Ω_0 (in absolute value), the actuator goes into dry friction mode with lower

friction torque (phenomenon of *stiction*). We observe here that discontinuity no longer occurs at the speed level, but at the level of friction torque, which is not representative of the energy. Consequently, this discontinuity is admissible, and is in fact an idealized vision of the Striebeck friction (Figure 7.2).

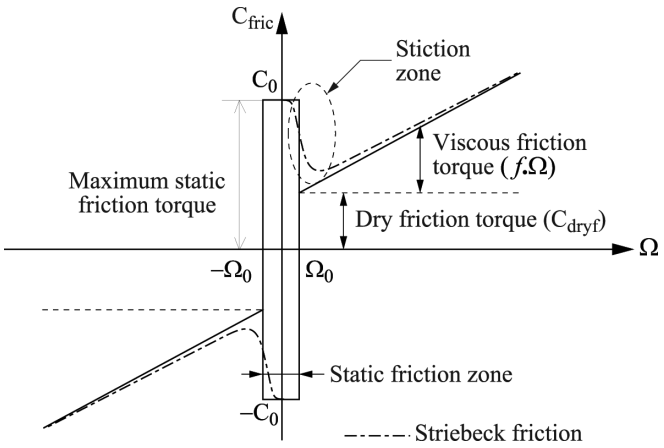

Figure 7.2. *Combination of friction models*

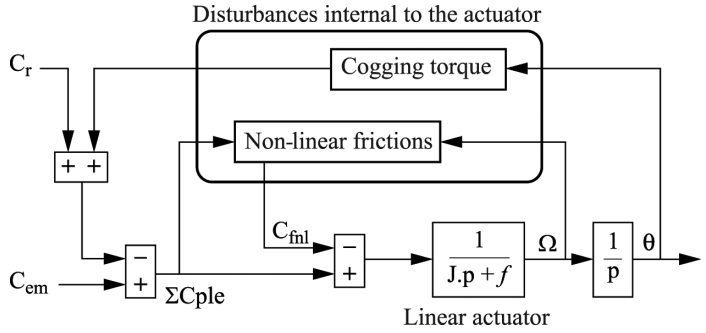

Figure 7.3. *Consideration of disturbances internal to the actuator*

In braking phase, reasoning is the same. When speed becomes lower than Ω_0 (in absolute value), the actuator goes from dry friction mode to static friction mode. The slowdown thus becomes more important. When speed is zero, we are then in real static friction conditions as described earlier. $|\Sigma Cple|$ must pass C_0 once more so that the actuator can start moving. In simulation, it is difficult to find a speed that is exactly zero once the calculations are launched. Because of this, the simulated

actuator may show an oscillation around zero speed, which does not correspond to reality [FÖR 95]. To avoid this phenomenon, we propose canceling the torque at linear actuator input when the speed is in a range close to zero, or $|\Omega| < 0.05\Omega_0$, for example. This cancelation is obtained by making C_{fnl} equal to $\Sigma Cple$, if $|\Sigma Cple|$ is lower than C_0. If $|\Sigma Cple|$ is higher than C_0, there is no torque cancelation at linear actuator input, and we must then apply equation [7.5] as long as the speed is close to zero. If speed is higher than $0.05\Omega_0$, equation [7.6] applies. The cancelation of torque at linear actuator input comes down to letting the actuator evolve according to its dampened free mode from initial conditions that were almost zero; speed can therefore be considered as zero.

The mechanical equation corresponding to the cancelation of the torque at linear actuator input is close to [7.4] and is written as:

$$J \cdot \frac{\mathrm{d}\Omega}{\mathrm{d}t} = -f \cdot \Omega \approx 0 \quad \text{with} \quad |\Omega| < 0.05 \cdot \Omega_0 \qquad [7.7]$$

It seems obvious that this speed range is contained in the static friction range. The torque cancelation at linear actuator input is thus equivalent to being in ideal static friction conditions ($\Omega = 0$) when $|\Sigma Cple| < C_0$ [7.4]. The previous considerations lead Figure 7.4, which can be implemented in simulation software such as SIMULINK™.

7.3. Modal control of the actuator with load torque observation

7.3.1. *Introduction*

The behavior of a position variable speed drive depends not only on the control law used but also on the powered load. During the definition of the control law, we mainly focus on its dynamic behavior in terms of variations of the set point, whereas the influence of the load torque is only rarely taken into consideration. And yet, its effect modifies the behavior of the variable speed drive by creating significant disturbances. To avoid this phenomenon, it may seem beneficial to compensate the load torque at control law level. The implementation of a sensor for the load torque is generally tricky and expensive. On the other hand, the implementation of an observer seems a profitable solution in many respects. This methodology obviously goes through a study of observability. The goal is to determine whether the variables used for the construction of the observation are sufficient, or in other words, whether the desired information is present in the measures that we allow ourselves.

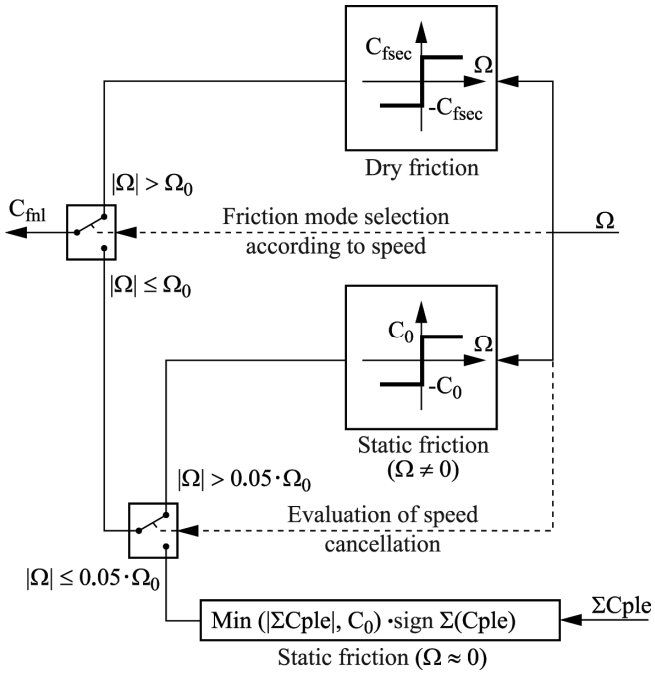

Figure 7.4. *Simulation diagram of non-linear friction*

7.3.2. *State representation of the actuator*

The state equation of the actuator comes from the mechanical equation of the motor:

$$J \cdot \frac{\mathrm{d}\Omega}{\mathrm{d}t} = C_{\mathrm{em}} - f \cdot \Omega - C_{\mathrm{r}} \text{ with } C_{\mathrm{em}} = K_{\mathrm{em}} \cdot I \qquad [7.8]$$

The parameters and variables used in this equation are:

J: inertia of the motor and its load;

f: friction factor;

Ω: mechanical speed;

C_{r}: load torque;

C_{em}: motor torque;

K_{em}: constant of torque;

I: rms value of three-phase currents feeding the motor.

Since the inverter is assimilated to a perfect current source, the current is a variable that is infinitely quick in relation to speed. State variables are speed Ω and position θ.

From [7.8], the state equation of the actuator is:

$$\begin{pmatrix} \dot{\Omega} \\ \dot{\theta} \end{pmatrix} = \begin{bmatrix} -\frac{f}{J} & 0 \\ 1 & 0 \end{bmatrix} \cdot \begin{pmatrix} \Omega \\ \theta \end{pmatrix} + \begin{bmatrix} \frac{K_{em}}{J} \\ 0 \end{bmatrix} \cdot I + \begin{bmatrix} \frac{-1}{J} \\ 0 \end{bmatrix} \cdot C_r \qquad [7.9]$$

$$\underline{\dot{X}} = A \cdot \underline{X} + B_m \cdot I + B_v \cdot C_r$$

The discretization of this system to sampling period T_e [BÜH 83] leads to:

$$\begin{aligned} \underline{X}\left((k+1)\cdot T_e\right) = e^{A\cdot T_e} = \underline{X}\left[k\cdot T_e\right] \quad &+ \quad \int_{k\cdot T_e}^{(k+1)\cdot T_e} e^{A\cdot\left((K+1)\cdot T_e-\tau\right)} \cdot B_m \cdot I(\tau)\,d\tau \\ &+ \quad \int_{k\cdot T_e}^{(k+1)\cdot T_e} e^{A\cdot\left((K+1)\cdot T_e-\tau\right)} \cdot B_v \cdot C_r(\tau)\,d\tau \end{aligned} \qquad [7.10]$$

The matrix exponential is calculated by using the theory of matrix functions [GAN 66, ROT 95]:

$$F_m = e^{A\cdot T_e} = \begin{bmatrix} \lambda & 0 \\ \frac{J}{f}\cdot(1-\lambda) & 1 \end{bmatrix} = \begin{bmatrix} F_{m11} & 0 \\ F_{m21} & 1 \end{bmatrix} \quad \text{with} \quad \lambda = e^{-\frac{f}{J}T_e} \qquad [7.11]$$

Control variable $I(\tau)$ remains constant during the sampling period. This is perfectly well represented by the zero-order relay. Assuming that $C_r(\tau)$ remains as constant is more doubtful because the load torque is independent of the control law, and can, therefore, vary between two sampling moments. However, this hypothesis is nevertheless accepted if the sampling period is small compared with the mechanical time constant. Hence, from [7.11]:

$$H_m = e^{A\cdot(k+1)\cdot T_e} \cdot \int_{k\cdot T_e}^{(k+1)\cdot T_e} e^{-A\cdot\tau} \cdot d\tau \cdot B_m = \begin{bmatrix} \frac{K_{em}}{f}\cdot(1-\lambda) \\ \frac{K_{em}}{f}\cdot\left(T_e - \frac{J}{f}\cdot(1-\lambda)\right) \end{bmatrix} = \begin{bmatrix} H_{m1} \\ H_{m2} \end{bmatrix} \qquad [7.12]$$

$$H_{\mathrm{m}} = \mathrm{e}^{A\cdot(k+1)\cdot T_{\mathrm{e}}} \cdot \int_{k\cdot T_{\mathrm{e}}}^{(k+1)\cdot T_{\mathrm{e}}} \mathrm{e}^{-A\cdot\tau} \cdot \mathrm{d}\tau \cdot B_{\mathrm{v}} = \begin{bmatrix} \dfrac{-1}{f}\cdot(1-\lambda) \\ \dfrac{-1}{f}\cdot\left(T_{\mathrm{e}} - \dfrac{J}{f}\cdot(1-\lambda)\right) \end{bmatrix} = \begin{bmatrix} H_{\mathrm{v1}} \\ H_{\mathrm{v2}} \end{bmatrix} \qquad [7.13]$$

From relations [7.12] and [7.13], we have:

$$-\frac{1}{K_{\mathrm{em}}} = \frac{H_{\mathrm{v1}}}{H_{\mathrm{m1}}} = \frac{H_{\mathrm{v2}}}{H_{\mathrm{m2}}} \Leftrightarrow H_{\mathrm{v1}} \cdot H_{\mathrm{m2}} = H_{\mathrm{m1}} \cdot H_{\mathrm{v2}} \qquad [7.14]$$

Hence, the discrete state equation:

$$\begin{pmatrix} \Omega(k+1) \\ \theta(k+1) \end{pmatrix} = \begin{bmatrix} F_{\mathrm{m11}} & 0 \\ F_{\mathrm{m21}} & 1 \end{bmatrix} \cdot \begin{pmatrix} \Omega(k) \\ \theta(k) \end{pmatrix} + \begin{bmatrix} H_{\mathrm{m1}} \\ H_{\mathrm{m2}} \end{bmatrix} \cdot I(k) + \begin{bmatrix} H_{\mathrm{v1}} \\ H_{\mathrm{v2}} \end{bmatrix} \cdot C_{\mathrm{r}}(k) \qquad [7.15]$$

7.3.3. *Analysis of controllability and observability*

Before implementing a control law by state feedback, we must make sure of system controllability, in order to act on both state variables by the control dimension $I(k)$. We use the Kalman criterion on the controllability matrix:

$$Q_{\mathrm{c}} = \begin{bmatrix} H_{\mathrm{m}} & F_{\mathrm{m}} \cdot H_{\mathrm{m}} \end{bmatrix} = \begin{bmatrix} H_{\mathrm{m1}} & \lambda \cdot H_{\mathrm{m1}} \\ H_{\mathrm{m2}} & \dfrac{J}{f}(1-\lambda)\cdot H_{\mathrm{m1}} + H_{\mathrm{m2}} \end{bmatrix} \qquad [7.16]$$

It must be of the second order, or its determinant must not be zero:

$$\det(Q_{\mathrm{c}}) = H_{\mathrm{m1}}^2 \cdot T_{\mathrm{e}} \neq 0 \quad \text{because} \quad T_{\mathrm{e}} \neq 0 \quad \text{and} \quad \lambda \neq 1 \qquad [7.17]$$

The system is, therefore, controllable. The study of observability is carried out in a similar way with the help of the Kalman criterion. The object is to verify that the order of the matrix of observability is equal to the sequence of the system. The matrix of observability depends on the output, which is either speed or position. If its output is position:

$$\theta(k) - C_{\mathrm{m}} \cdot \underline{X} = \begin{bmatrix} 0 & 1 \end{bmatrix} \cdot \begin{pmatrix} \Omega(k) \\ \theta(k) \end{pmatrix} \qquad [7.18]$$

The matrix of observability is then equal to:

$$Q_o = \begin{bmatrix} C_m \\ C_m \cdot F_m \end{bmatrix} = \begin{bmatrix} 0 & 1 \\ \frac{J}{f} \cdot (1-\lambda) & 1 \end{bmatrix} \quad [7.19]$$

and determinant of Q_o is different of zero:

$$\det(Q_o) = \frac{J}{f} \cdot (\lambda - 1) \neq 0 \quad \text{because} \quad \lambda \neq 1 \quad \text{since} \quad (T_e \neq 0) \quad [7.20]$$

The system is therefore observable for position and state feedback (speed and position) is possible for the measure of position.

If the output is speed:

$$C_m = \begin{bmatrix} 1 & 0 \end{bmatrix} \quad \text{and} \quad \det(Q_o) = \begin{vmatrix} 1 & 0 \\ \lambda & 0 \end{vmatrix} = 0 \quad [7.21]$$

The system is therefore not observable from the measure of speed. In fact, the integration of speed only provides information on the position variation and not on initial position. The state feedback from the measure of speed is possible if the initial position is known. This study of observability will be discussed in section 7.4.

7.3.4. *Control law by state feedback*

The system is controllable (section 7.3.3) and state variables are presumed measurable by sensors. We first present the control structure, followed by the sizing of its parameters and finally a method of limitation for the integral action, connected to the limitation with current set point I_{ref}.

7.3.4.1. *Control structure*

Control (Figure 7.5) contains a state feedback on state variables, speed Ω and position θ with gains K_{s1} and K_{s2}. We choose the "optimal state adjustment structure" defined by Bühler [BÜH 83], by adding three actions:

– an integral action to cancel the error position in steady state operation, as because of non-linearities (dry friction, etc.), the integration between position and speed is not sufficient. Integrator X_r's input is affected by a gain K_r;

– a load torque compensation with gain K_v;

– a term proportional to the set point that acts on control I with gain K_θ, which accelerates the response to the position set point, by bringing a zero in the equivalent transfer function between input and output.

A current set point limitation provided for the inverter is necessary to ensure the security of the variable speed drive. This limitation requires a limitation of the integral action.

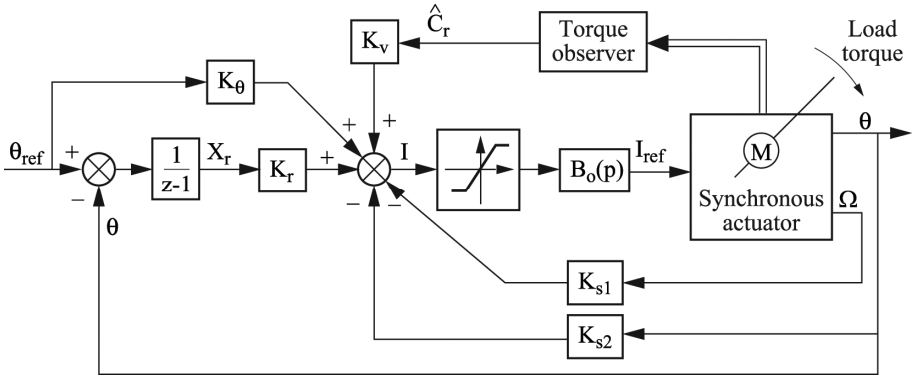

Figure 7.5. *Optimal structure of state setting*

7.3.4.2. *Sizing of the control law*

The sizing of the control law is achieved by the determination of the five gains. First, we define the state feedback and integral action (K_{s1}, K_{s2} and K_r) gains by the choice of closed-loop poles that set the dynamic. Then we calculate the compensation gain of load torque (K_v) to cancel the influence of the load torque on position. Finally, we define the gain linked to set point (K_θ) according to the desired dynamic behavior in uni-set response or path following. In order to achieve this sizing, we define the closed-loop state equation from equation [7.15] and the equations of control algorithm [7.22] and [7.23]:

$$X_r(k+1) = X_r(k) + \theta_{ref}(k) - \theta(k) \qquad [7.22]$$

$$I(k) = -K_{s1} \cdot \Omega(k) - K_{s2} \cdot \theta(k) + K_r \cdot X_r(k) + K_\theta \cdot \theta_{ref}(k) + K_v \cdot \hat{C}_r(k) \qquad [7.23]$$

$X_r(k)$ is the third state variable, and by combining [7.15], [7.22] and [7.23], we get closed-loop state equations:

$$\begin{pmatrix} \Omega(k+1) \\ \theta(k+1) \\ X_r(k+1) \end{pmatrix} = \begin{bmatrix} F_{m11} - H_{m1} \cdot K_{s1} & -H_{m1} \cdot K_{s2} & H_{m1} \cdot K_r \\ F_{m21} - H_{m2} \cdot K_{s1} & 1 - H_{m2} \cdot K_{s2} & H_{m2} \cdot K_r \end{bmatrix} \cdot \begin{pmatrix} \Omega(k) \\ \theta(k) \\ X_r(k) \end{pmatrix} + \begin{bmatrix} H_{m1} \cdot K_\theta \\ H_{m2} \cdot K_\theta \end{bmatrix} \cdot \theta_{ref}(k) + \begin{bmatrix} H_{v1} \\ H_{v2} \\ 0 \end{bmatrix} \cdot C_r(k) + \begin{bmatrix} H_{m1} \cdot K_v \\ H_{m2} \cdot K_v \\ 0 \end{bmatrix} \cdot \hat{C}_r(k) \quad [7.24]$$

$$F_{bf} = \begin{bmatrix} F_{m11} - H_{m1} \cdot K_{s1} & -H_{m1} \cdot K_{s2} & H_{m1} \cdot K_r \\ F_{m21} - H_{m2} \cdot K_{s1} & 1 - H_{m2} \cdot K_{s2} & H_{m2} \cdot K_r \\ 0 & -1 & 1 \end{bmatrix} \quad [7.25]$$

If its output is position:

$$C_m = \begin{bmatrix} 1 & 0 & 0 \end{bmatrix}$$

– *Pole placement*: Coefficients of F_{bf} [7.25] determine the closed-loop dynamic of the actuator and depend on the gains from the control law (K_{s1}, K_{s2} and K_r). The calculation of K_{s1}, K_{s2} and K_r is done by the identification of the polynomial characteristic of F_{bf} with a same order polynomial characterizing the desired dynamic. We choose a real triple pole p_{bf} in order to avoid possible overshoots.

Characteristic polynomial:

$$\det\left(z \cdot 1 - F_{bf}\right) \quad \text{with} \quad 1, \text{ identity matrix} \quad [7.26]$$

Desired polynomial:

$$\left(z - p_{bf}\right)^3 \quad \text{with} \quad p_{bf} = e^{-T_e \cdot \omega_{bf}} \quad [7.27]$$

ω_{bf} corresponds to the bandwidth equivalent to p_{bf} in the continuous field. Since the pole is triple, the bandwidth is defined from an attenuation of 9 dB.

We get:

$$K_{\mathrm{r}} = \frac{\left(1 - p_{\mathrm{bf}}\right)^3}{F_{\mathrm{m21}} \cdot H_{\mathrm{m1}} - F_{\mathrm{m11}} \cdot H_{\mathrm{m2}} + H_{\mathrm{m2}}}$$

$$K_{\mathrm{s1}} = \left(F_{\mathrm{m11}} - p_{\mathrm{bf}}^3 + \left(F_{\mathrm{m21}} \cdot H_{\mathrm{m1}} - F_{\mathrm{m11}} \cdot H_{\mathrm{m2}} \right) \left(\frac{2 + F_{\mathrm{m11}} - 3 \cdot p_{\mathrm{bf}}}{H_{\mathrm{m2}}} - K_{\mathrm{r}} \right) \right) \times \frac{H_{\mathrm{m2}}}{H_{\mathrm{m1}} \cdot \left(F_{\mathrm{m21}} \cdot H_{\mathrm{m1}} - F_{\mathrm{m11}} \cdot H_{\mathrm{m2}} + H_{\mathrm{m2}} \right)}$$

$$K_{\mathrm{s2}} = \frac{2 + F_{\mathrm{m11}} - 3 \cdot p_{\mathrm{bf}} - H_{\mathrm{m1}} \cdot K_{\mathrm{s1}}}{H_{\mathrm{m2}}} \qquad [7.28]$$

– *Determination of* K_{v}: the compensation gain of the resistant torque (K_{v}) is calculated from [7.24],

$$\begin{pmatrix} \Omega(k+1) \\ \theta(k+1) \\ X_{\mathrm{r}}(k+1) \end{pmatrix} = \left[F_{\mathrm{bf}} \right] \cdot \begin{pmatrix} \Omega(k) \\ \theta(k) \\ X_{\mathrm{r}}(k) \end{pmatrix} + \begin{pmatrix} H_{\mathrm{m1}} \cdot K_{\theta} \\ H_{\mathrm{m2}} \cdot K_{\theta} \\ 1 \end{pmatrix} \cdot \theta_{\mathrm{ref}}(k) + \begin{bmatrix} H_{\mathrm{v1}} + H_{\mathrm{m1}} \cdot K_{\mathrm{v}} \\ H_{\mathrm{v2}} + H_{\mathrm{m2}} \cdot K_{\mathrm{v}} \\ 0 \end{bmatrix} \cdot C_{\mathrm{r}}(k) \qquad [7.29]$$

To cancel the load torque effect and by considering [3.14], K_{v} is chosen in such a way that:

$$K_{\mathrm{v}} = \frac{H_{\mathrm{v1}}}{H_{\mathrm{m1}}} \quad \text{and} \quad K_{\mathrm{v}} = -\frac{H_{\mathrm{v2}}}{H_{\mathrm{m2}}} \quad \text{either} \quad K_{\mathrm{v}} = \frac{1}{K_{\mathrm{em}}} \qquad [7.30]$$

Term $K_{\mathrm{v}} \cdot \hat{C}_{\mathrm{r}}(k)$ in the control law corresponds to the equivalent current that must be added at the current set point to compensate the load torque. However, this compensation is not perfect because the observer dynamic is not infinite.

– *Determination of* K_{θ} : K_{θ} can be defined in two ways:

- the first one consists of compensating a transfer function pole between position and position set point [7.31] by the zero displaceable by K_{θ}, to improve the dynamic behavior in relation of set point changes. This zero, which is equal to $1 - K_{\mathrm{r}} / K_{\theta}$, can lead to unfortunate overshoots:

$$\frac{\theta(z)}{\theta_{\text{ref}}(z)} = \left[C_{\text{m}}\right]\cdot \text{Adj}\left(z\cdot 1 - F_{\text{bf}}\right)\cdot \begin{bmatrix} H_{\text{m1}}\cdot K_\theta \\ H_{\text{m2}}\cdot K_\theta \\ 1 \end{bmatrix}$$
$$= \frac{K_\theta \cdot \left(z - 1 + \dfrac{K_{\text{r}}}{K_\theta}\right)\cdot\left(H_{\text{m2}}\cdot z - F_{\text{m11}}\cdot H_{\text{m2}} + F_{\text{m21}}\cdot H_{\text{m1}}\right)}{\det\left(z\cdot 1 - F_{\text{bf}}\right)} \qquad [7.31]$$

To compensate a pole p_{bf}:

$$1 - \frac{K_{\text{r}}}{K_\theta} = p_{\text{bf}} \quad \text{or} \quad K_\theta = \frac{K_{\text{r}}}{1 - p_{\text{bf}}} \qquad [7.32]$$

K_{r} is imposed by the pole placement, and the closed-loop transmittance becomes:

$$\frac{\theta(z)}{\theta_{\text{ref}}(z)} = \frac{K_{\text{r}}}{1 - p_{\text{bf}}}\cdot\frac{\left(H_{\text{m2}}\cdot z - F_{\text{m11}}\cdot H_{\text{m2}} + F_{\text{m21}}\cdot H_{\text{m1}}\right)}{\left(z - p_{\text{bf}}\right)^2} \qquad [7.33]$$

- the second one consists of canceling the output of the sinusoidal mode integrator, and it is only efficient if the load torque is zero or compensated. Otherwise, the integral action compensates the load torque and the integral action output is no longer zero in sinusoidal mode. K_θ is defined by considering the sinusoidal mode reached. From [7.24] in sinusoidal mode, we have:

$$\Omega(k+1) = \Omega(k) = 0 \quad \text{and} \quad \theta(k+1) = \theta(k) = \theta_{\text{ref}}(k)$$
$$\Downarrow \qquad [7.34]$$
$$H_{\text{m1}}\cdot\left(K_\theta - K_{\text{s2}}\right)\cdot\theta_{\text{ref}}(k) + H_{\text{m1}}\cdot K_{\text{r}}\cdot X_{\text{r}}\left(k\right) = 0$$

where

$$K_\theta = K_{\text{s2}} \qquad [7.35]$$

K_{s2} is determined by pole placement. The closed-loop transfer function is:

$$\frac{\theta(z)}{\theta_{\text{ref}}(z)} = \frac{\left(K_{\text{s2}}\cdot z - K_{\text{s2}} + K_{\text{r}}\right)\cdot\left(H_{\text{m2}}\cdot z - F_{\text{m11}}\cdot H_{\text{m2}} + F_{\text{m21}}\cdot H_{\text{m1}}\right)}{\left(z - p_{\text{bf}}\right)^3} \qquad [7.36]$$

Experimental results (Figure 7.6) show the influence of K_θ on the step response of the actuator. The second method, contrary to the first one, creates an overshoot that

can be damaging, but inevitable if we want to cancel X_r in steady state operation, when the set point is constant. On the other hand, this same method makes it possible to cancel the velocity error for a side input.

With $K_\theta = K_{s2}$ (cancelation of integrator output), the new diagram (Figure 7.7) clarifies the sampled transfer function. We have a particular cascade structure, since the integral action is in the external loop (position) and not in the internal loop (speed) as is traditionally the case. The integrator output is zero in steady-state operation ($\theta = \theta_{ref}$ and $\Omega = 0$), only if the load torque is compensated or zero.

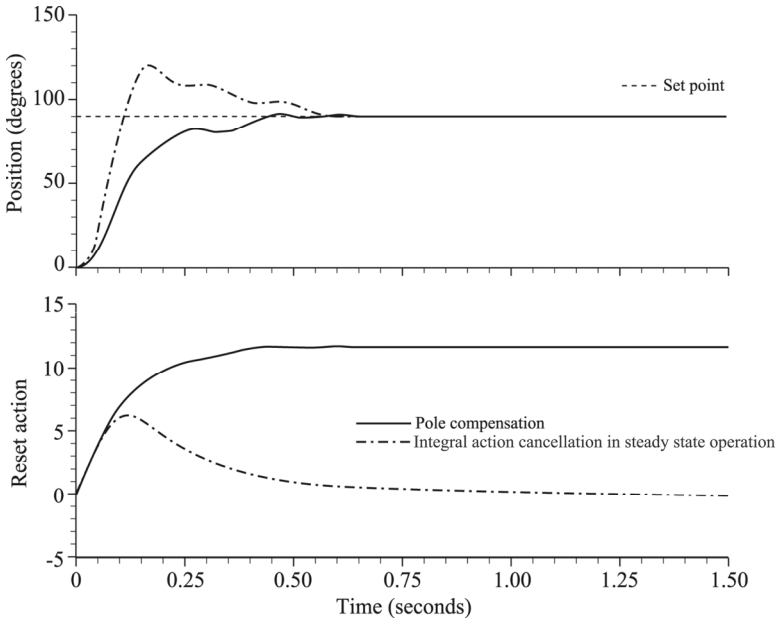

Figure 7.6. *Influence of the K_θ choice on the step response of the actuator (experimental results)*

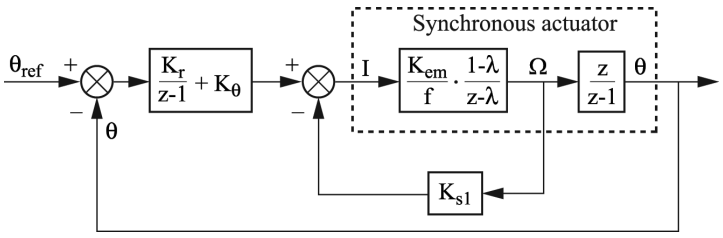

Figure 7.7. *Structure of control law with $K_\theta = K_{s2}$*

Because of the two integrations (control law and physical integration) in the action chain, the velocity error for a ramp input is zero. In order to evaluate it, the velocity error is calculated when coefficients K_{s2} and K_θ are not equal. From [7.24], we have:

$$\frac{\theta(z)}{\theta_{ref}(z)} = C_m.\left[z \cdot 1 - F_{bf}\right]^{-1}.\begin{bmatrix} H_{m1} \cdot K_\theta \\ H_{m2} \cdot K_\theta \\ 1 \end{bmatrix} \quad [7.37]$$

The error on position is:

$$\varepsilon_\theta(z) = \theta_{ref}(z) - \theta(z) = \left(1 - \frac{\theta(z)}{\theta_{ref}(z)} \cdot \theta_{ref}(z)\right) \quad [7.38]$$

With the theorem of the final value, for a (gradient b) ramp input, we have:

$$\varepsilon_\theta(\infty) = \lim_{z \to 1}\left(\frac{z-1}{z} \cdot \left(1 - \frac{\theta(z)}{\theta_{ref}(z)}\right) \cdot \theta_{ref}(z)\right)$$

$$\text{with } \theta_{ref}(z) = b \cdot \frac{T_e \cdot z}{(z-1)^2} \quad [7.39]$$

$$\varepsilon_\theta(\infty) = b \cdot T_e \cdot \frac{K_{s2} - K_\theta}{K_r}$$

The velocity error [7.39] for a ramp input is zero when $K_{s2} = K_\theta$. Otherwise, it is constant and depends on the ramp gradient given in set point. The steady state operation error is always zero for a set point in pole step, regardless of the choice of K_θ.

In experimental tests (Figure 7.8), the velocity error is zero when the reset action is canceled in steady state operation. Error fluctuations around zero are attributed to the machine's slot torque. When zero is compensated, the velocity error is constant [7.39]. Experimental conditions are as follows and correspond to a triple pole placement:

ω_{bf} = 15 rad/s (p_{bf} = 0.74);

K_{s2} = 5.7379; b = 360°/s;

K_θ = 1.9996; T_e = 20 ms;

K_r = 0.5183.

Error [7.39] equals: $\varepsilon_\theta(\infty)$ = 51.9°. This result reflects the velocity error experimentally sampled at approximately 50°.

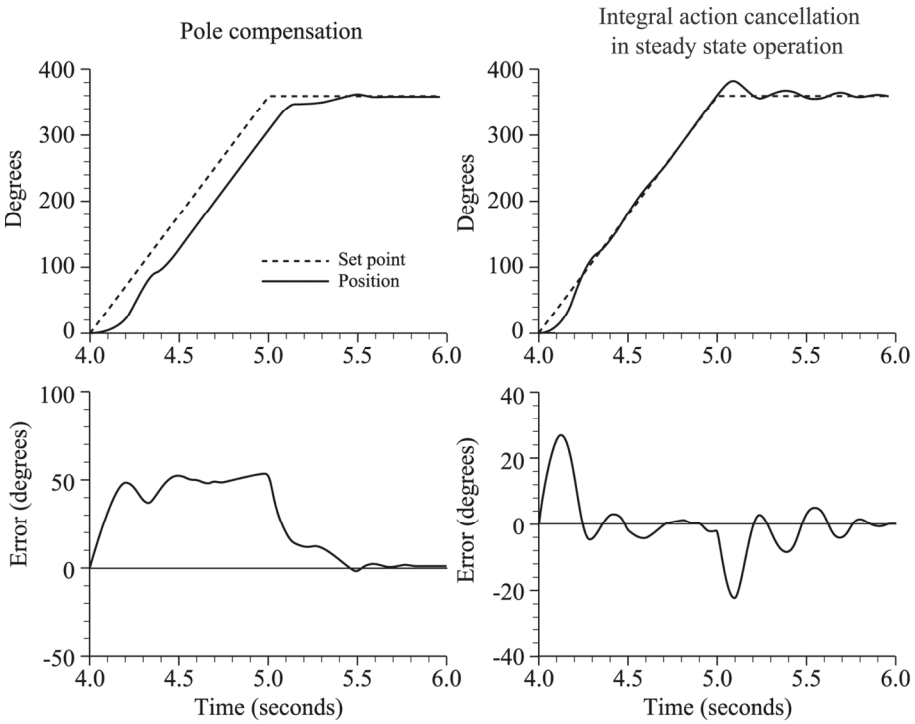

Figure 7.8. *Influence of the choice of K_θ on actuator response at a ramp input (experimental results)*

7.3.4.3. *Limitation of the integral action*

The limitation of control variable I_{ref} requires a limitation of the integral action. This control limitation slows down the system and the error does not decrease according to the control dynamic. Without limitation, the integrator triggers an excessive overshoot of the output variable. Digitally, this overshoot problem is all the more significant as the number of bits used for programming variables is high (32 bits in our case).

The limitation of X_r avoids this "drift". The procedure recalculates the reset component, according to the control limit value (I_{lim}) and operating conditions [BÜH 82]:

$$X_r(k) = \frac{I_{lim}(k) + K_{s1} \cdot \Omega(k) + K_{s2} \cdot \theta(k) - k_\theta \cdot \theta_{ref}(k)}{K_r} \qquad [7.40]$$

The effect of limitation is shown in an experimental test (Figure 7.9). The position no longer has an overshoot and also benefits from better response time. In addition, control is not saturated as long, decreasing the constraint (maximum intensity time) experienced by the variable speed drive. The second gradient shows the evolution of the integral action in limitation phase.

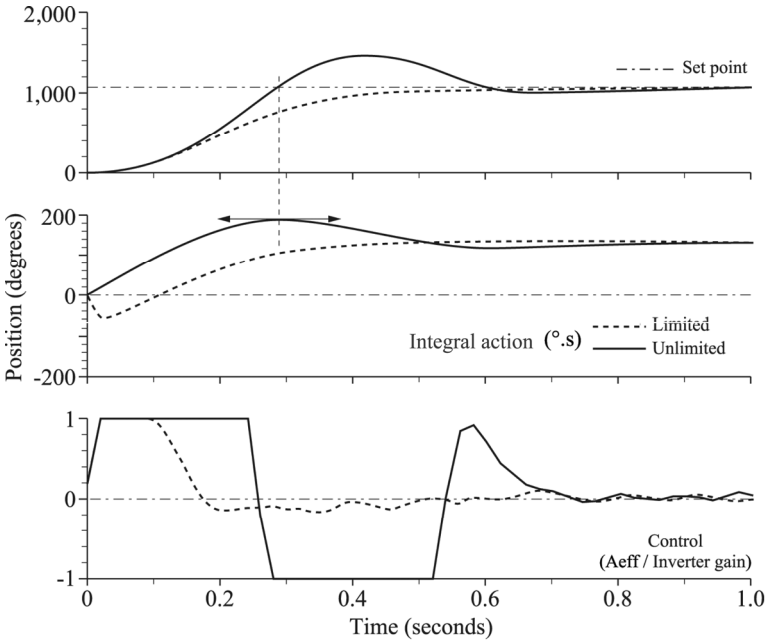

Figure 7.9. *Influence of integral action limitation (experimental results)*

This limitation method seems the simplest to use. There are others based on retro-propagation of maximum references [WES 94] or on a change in the regulation structure in case of limitation [BÜH 88].

7.4. Observation of load torque

7.4.1. *Introduction*

The behavior of a position variable speed drive depends not only on the type of control law used but also on the load drive. During the definition of the control law, we mainly focus on its dynamic behavior in terms of variations of the set point, whereas the influence of the load torque is only rarely taken into consideration. And yet, its effect modifies the variable speed drive behavior and the position no longer

depends exclusively on the set point. To avoid this phenomenon, we must compensate the resistant torque at the level of the control law. Since the measure of load torque with a sensor is generally tricky and expensive, a resistant torque observer can be implemented.

First, we consider a simple type of observer called "observer with loop integration", and its performance will be analyzed with the help of simulations.

Second, we develop several state observation structures that will be compared. In order to implement the load torque observer, the actuator state vector is increased by an additional variable, the load torque. The observation structures described in this section are different in their sequence and variables used (speed or position) to ensure observer convergence. For each structure, the analysis of the transfer function between the observed and real torque determines its performances. The observation error of measurable state variables is evaluated. This evaluation is done from transfer functions linking the state variables of the actuator and those from the observer to the system's input variables. The most interesting experimental results of observation structures are presented.

7.4.2. *Observer with integration in the loop*

7.4.2.1. *Principle*

The reconstruction of the load torque can be obtained by integrating the speed error caused by the difference between the measured speed and the speed taken from a model (Figure 7.10). This technique was often experienced [LEP 93] for this purpose and for the estimation of a system's parameter.

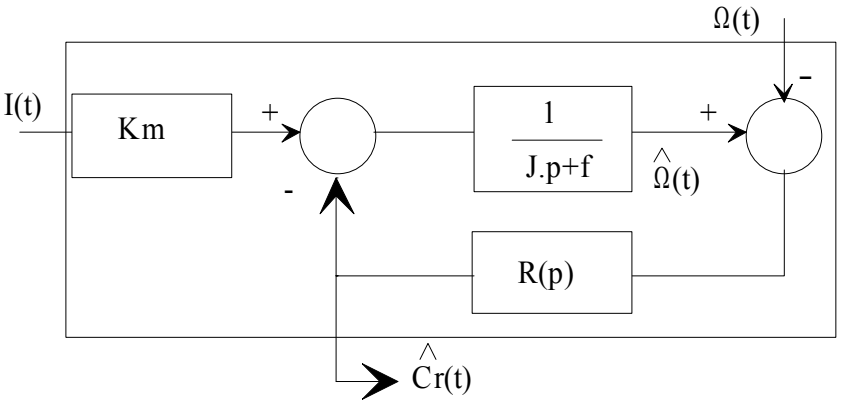

Figure 7.10. *Diagram of principle of an observer with integration*

The regulator makes the speed error lean toward zero and converge the estimated load torque toward the real load torque: load drive and/or internal machine torque (cogging torque).

The regulator parameters are defined by a pole placement imposing a desired dynamic.

Because of the simplicity of the system, the regulator is chosen proportionally integral:

$$R(p) = \frac{K_{\mathrm{p}} \cdot p + K_{\mathrm{i}}}{p} \qquad [7.41]$$

Put into an equation:

$$\begin{bmatrix} \dot{\hat{\Omega}} \\ \dot{x}_{\mathrm{r}} \end{bmatrix} = \begin{bmatrix} -\dfrac{f + K_{\mathrm{p}}}{J} & -\dfrac{K_{\mathrm{i}}}{J} \\ 1 & 0 \end{bmatrix} \cdot \begin{bmatrix} \hat{\Omega} \\ x_{\mathrm{r}} \end{bmatrix} + \begin{bmatrix} \dfrac{K_{\mathrm{m}}}{J} & \dfrac{K_{\mathrm{p}}}{J} \\ 0 & -1 \end{bmatrix} \cdot \begin{bmatrix} I \\ \Omega \end{bmatrix} \qquad [7.42]$$

$$x_{\mathrm{r}} = \int \left(\hat{\Omega} - \Omega \right) \mathrm{d}t$$

$$\hat{C}_{\mathrm{r}} = \begin{bmatrix} K_{\mathrm{p}} & K_{\mathrm{i}} \end{bmatrix} \begin{bmatrix} \hat{\Omega} \\ x_{\mathrm{r}} \end{bmatrix} + \begin{bmatrix} 0 - K_{\mathrm{p}} \end{bmatrix} \cdot \begin{bmatrix} I \\ \Omega \end{bmatrix} \qquad [7.43]$$

By identifying with a second-order system $\left(\xi, \omega_{\mathrm{n}}\right)$, we obtain:

$$K_{\mathrm{p}} = 2 \cdot \xi \cdot \omega_{\mathrm{n}} \cdot J - f \quad \text{and} \quad K_{\mathrm{i}} = \omega_{\mathrm{n}}^2 \cdot J \qquad [7.44]$$

Torque reconstruction is characterized by the following transmittances:

$$\widehat{C}_{\mathrm{r}}(p) = T_1(p) * I(p) + T_2 * \Omega(p)$$

$$T_1(p) = \frac{\hat{C}_{\mathrm{r}}(p)}{I(p)} = \frac{K_{\mathrm{m}} \cdot (p \cdot K_{\mathrm{p}} + K_{\mathrm{i}})}{J \cdot p^2 + \left(K_{\mathrm{p}} + f\right) \cdot p + K_{\mathrm{i}}} = \frac{K_{\mathrm{m}} \cdot \left(p \cdot \sigma + \omega_{\mathrm{n}}^2\right)}{p^2 + 2 \cdot \xi \cdot \omega_{\mathrm{n}} \cdot p + \omega_{\mathrm{n}}^2}$$

$$\sigma = \left(2 \cdot \xi \cdot \omega_{\mathrm{n}} - \frac{f}{J} \right)$$

and

$$\begin{aligned} T_2(p) &= \frac{\hat{C}_{\mathrm{r}}(p)}{\Omega(p)} = -\frac{p^2 \cdot K_{\mathrm{p}} + p \cdot \left(K_{\mathrm{i}} \cdot J + K_{\mathrm{p}} \cdot f\right) + K_{\mathrm{i}} \cdot f}{J \cdot p^2 + \left(K_{\mathrm{p}} + f\right) \cdot p + K_{\mathrm{i}}} \\ &= -\frac{p^2 \cdot \sigma + p \cdot \left(J \cdot \omega_{\mathrm{n}}^2 + f \cdot \sigma\right) + \omega_{\mathrm{n}}^2 \cdot f}{p^2 + 2 \cdot \xi \cdot \omega_{\mathrm{n}} \cdot p + \omega_{\mathrm{n}}^2} \end{aligned} \quad [7.45]$$

We find the poles specified by doublet $\left(\xi, \omega_{\mathrm{n}}\right)$ and zero for $T_1(p)$, placed in:

$$\left(-\frac{J \cdot \omega_{\mathrm{n}}^2}{2 \cdot \xi \cdot \omega_{\mathrm{n}} \cdot J - f}\right)$$

That zero is directly caused by the regulator structure and can be positive if the dynamic imposed is too low. We will now analyze the behavior of this observer in an induction machine with strong cogging torque. It is a magnet machine with a quasi-sinusoidal electromotive form with the following characteristics:

– rated output: P = 1 kw;
– rated speed: N_{n} = 2,000 rpm;
– number of slots: N_{e} = 36;
– number of pole pairs: P_{p} = 2;
– inertia: $J = 2 \times 10^{-4}$ kg m^2;
– coefficient of viscous friction: $f = 9.3 \times 10^{-3}$ (Nm/rad/s);
– inductance: L = 0.48 mH;
– resistance: R = 2.75 Ω;
– coefficient of the cogging torque [2]: C_{d1} = 0.1; C_{d2} = 0.03; C_{d3} = 0.0016;
– harmonic coefficients: h_1 = 0.16 V/rad/s; h_3 = 1% of h_1;
– electromotive force: E = 250 V at rated speed;
– hysteresis control: H = 0.1 A;
– coefficient of torque: K_{em} = 0.65 Nm/A;
– I_{max} = 7.4 A a max torque of 4.8 Nm.

Simulation results at 700 rpm are illustrated in the following text and show the behavior of a resistant torque observer functioning on a permanent magnet machine with strong cogging torque.

7.4.2.2. *Open-loop operation*

Observer bandwidth must be defined with the consideration of the maximum rotation frequency and the number of slots. In fact, the frequency of ripples (Figure 7.11), linked to slots, corresponds to the power frequency multiplied by the number of slots, and the choice of angular frequency ω_n will be given accordingly as:

$$\omega_n > 2 \cdot \pi \cdot fsm \cdot \mathrm{Ne} \times 10$$

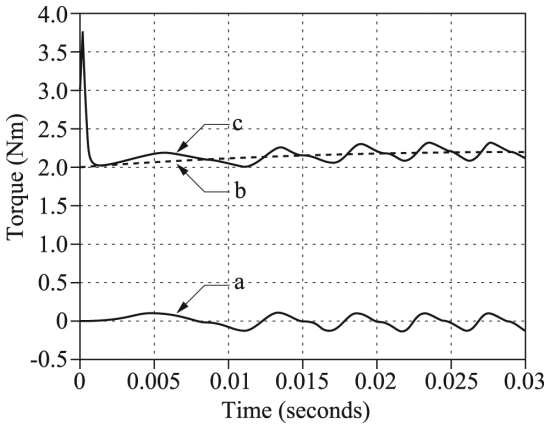

Figure 7.11. *(a) cogging torque; (b) applied load torque; (c) torque observer*

This observer uses the motor's mechanical parameters (inertia, friction factor, etc.), and it is important to evaluate the robustness of the observation in the presence of parametric variations.

The behavior of the observer is sensitive to the value of the friction factor, by introducing a bias (Figure 7.12). For inertia uncertainty, the observation dynamic is altered, but the average torque observed is correct in sinusoidal mode.

7.4.2.3. *Closed-loop operation*

We consider here a state feedback control defined continuously and using a compensation of the observed torque (Figure 7.13). The control law in closed loop imposes a triple pole with a value of $\omega_{bf} = 200\,\mathrm{rad/s}$, and the anticipation term is

used to compensate the pole by zero in order for the transfer function denominator to be at degree two in the closed loop. The gains are then expressed by:

$$K_{s1} = \frac{3 \cdot \omega_{bf} \cdot J - f}{K_m}, \quad K_{s2} = \frac{3 \cdot J \cdot \omega_{bf}^2}{K_m}, \quad K_r = \frac{J \cdot \omega_{bf}^3}{K_m}, \quad K_\theta = \frac{J \cdot \omega_{bf}^2}{K_m} \qquad [7.46]$$

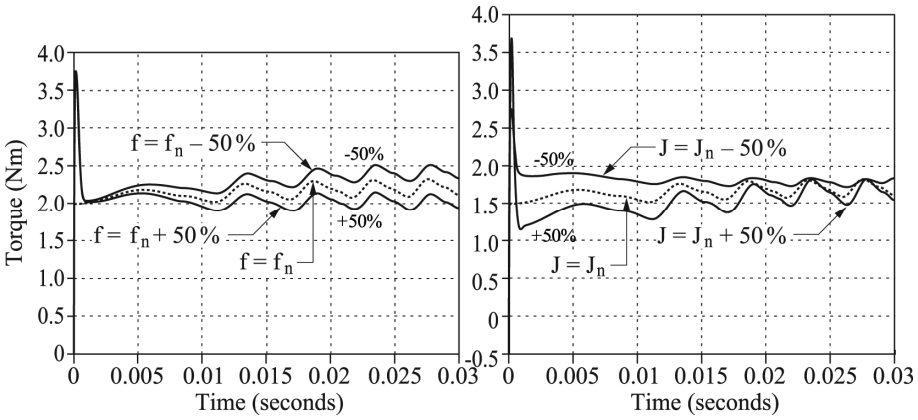

Figure 7.12. *Effects of J and f variations*

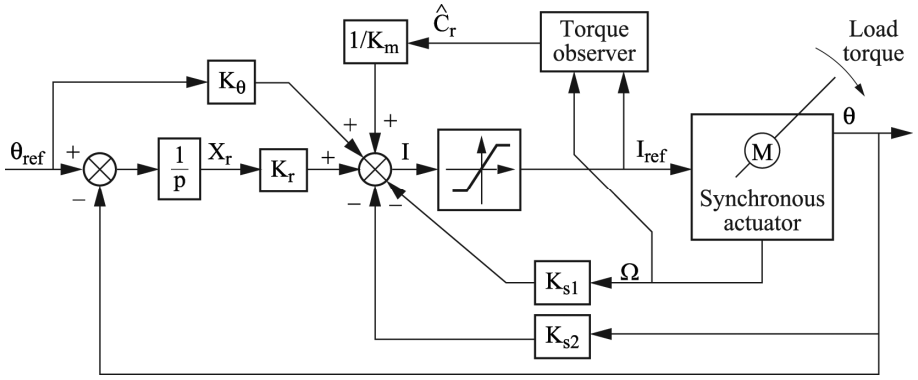

Figure 7.13. *Closed-loop control diagram*

The observer uses a PI regulator calculated to impose a double pole in $\omega_n = 300\,\text{rad/s}$. In Figure 7.14, the behavior of the variable speed drive is shown for a reference position step of 90° with a constant torque of 1 Nm applied at startup. This value is doubled from 0.06 s.

At moment $t = 0.09$ s, the position set point changes and the load torque remains the same.

With the help of the observer, the torque impact is only slightly noticeable (Figure 7.14), and the movement remains lower than 0.2°.

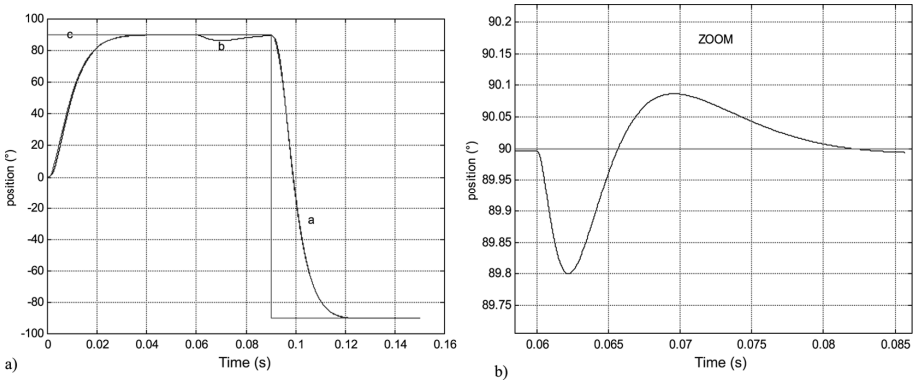

Figure 7.14. *Variable speed drive behavior in response to a set point step: (a) with observer; (b) without observer; (c) reference*

Figure 7.15 illustrates the behavior of the observer in abrupt variations of the torque applied to the machine as well as with the reconstruction of the cogging torque.

Since the mechanical load is not also perfectly known, it is interesting to learn more about the behavior of the observer in the presence of uncertainties in existing friction and powered inertia.

In the first series of simulations (Figure 7.16), we show the observed torque during a variation of the friction factor of ±50%.

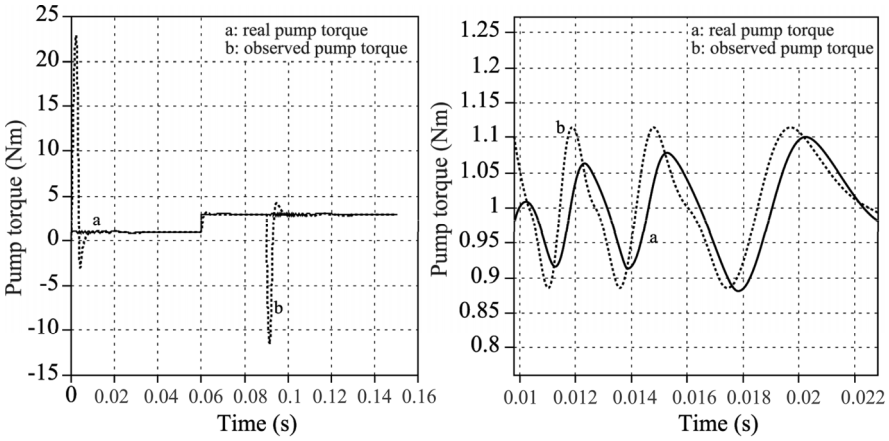

Figure 7.15. *Observed resistant torque*

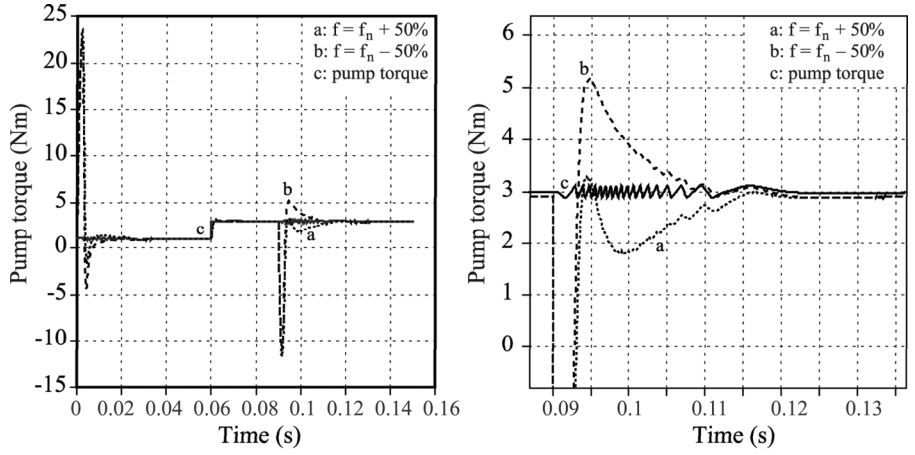

Figure 7.16.

These differences have very little influence on the evolution of the position that remains almost confused with nominal gradients. The evolution of the reference current (Figure 7.17) illustrates this small impact.

On the other hand, for a variation of inertia, the behavior is quite different, notably when inertia increases. In fact, strong amplitude oscillations emerge (Figure 7.18).

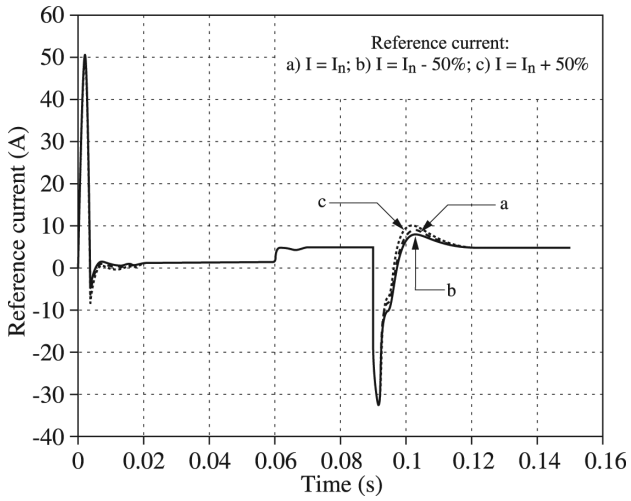

Figure 7.17.

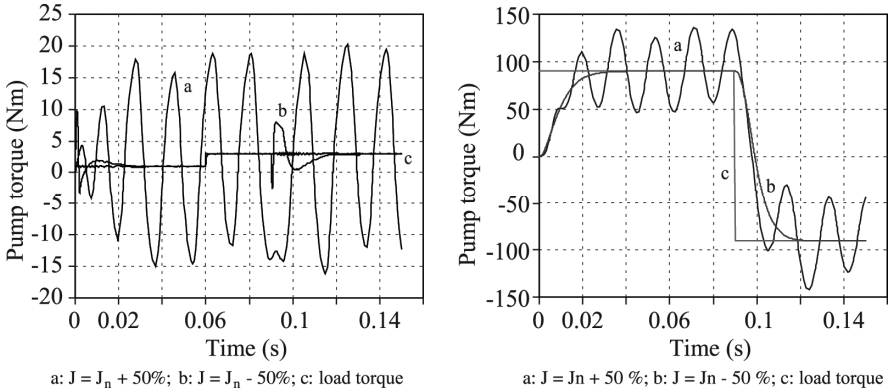

Figure 7.18.

For a decrease in inertia, sensitivity is low because the evolution of the position is only slightly affected.

7.4.2.4. *Analytical characterization*

The system made up of synchronous machine with its model, torque observer, control law, and torque compensation can be represented by a only state equation:

$$\begin{bmatrix} \dot{\Omega} \\ \dot{\Theta} \\ \dot{x}_{\mathrm{r}} \\ \dot{\Omega} \\ \dot{x}_{\mathrm{i}} \end{bmatrix} = \begin{bmatrix} -\frac{1}{J}\cdot\left(f + K_{\mathrm{m}}\cdot K_{\mathrm{s1}} - K_{\mathrm{p}}\right) & -\frac{1}{J}\cdot\left(K_{\mathrm{m}}\cdot K_{\mathrm{s2}}\right) & -\frac{1}{J}\cdot\left(K_{\mathrm{m}}\cdot K_{\mathrm{r}}\right) & -\frac{1}{J}\cdot\left(K_{\mathrm{p}}\right) & -\frac{1}{J}\cdot\left(K_{\mathrm{p}}\right) \\ 1 & 0 & 0 & 0 & 0 \\ 0 & -1 & 0 & 0 & 0 \\ -\frac{1}{J_0}\cdot\left(K_{\mathrm{mo}}\cdot K_{\mathrm{s1}}\right) & -\frac{1}{J_0}\cdot\left(K_{\mathrm{mo}}\cdot K_{\mathrm{s2}}\right) & -\frac{1}{J_0}\cdot\left(K_{\mathrm{mo}}\cdot K_{\mathrm{r}}\right) & -\frac{1}{J_0}\cdot\left(f_0\right) & 0 \\ -1 & 0 & 0 & 1 & 0 \end{bmatrix}$$

$$\cdot \begin{bmatrix} \Omega \\ \mathrm{Q} \\ x_{\mathrm{r}} \\ \hat{\Omega} \\ x_{\mathrm{i}} \end{bmatrix} + \begin{bmatrix} \frac{K_{\mathrm{m}}\cdot g}{J} & -\frac{1}{J} \\ 0 & 0 \\ 1 & 0 \\ \frac{K_{\mathrm{mo}}\cdot g}{J_0} & 0 \\ 0 & 0 \end{bmatrix} \cdot \begin{bmatrix} \Theta_{\mathrm{ref}} & C_{\mathrm{r}} \end{bmatrix} \qquad [7.47]$$

From this equation, the observed resistant torque is expressed by:

$$\hat{C}_{\mathrm{r}} = \begin{bmatrix} K_{\mathrm{p}} & 0 & 0 & -K_{\mathrm{p}} & K_{\mathrm{i}} \end{bmatrix} \begin{bmatrix} \Omega & \Theta & x_{\mathrm{r}} & \hat{\Omega} & x_{\mathrm{i}} \end{bmatrix}^{t} \qquad [7.48]$$

When the observer parameters are identical to those of the system, we can emphasize the transfer function of the observer:

$$G_1(p) = \frac{\hat{C}_{\mathrm{r}}(p)}{\Theta_{\mathrm{ref}}(p)} = 0 \qquad [7.49]$$

$$G_2(p) = \frac{\hat{C}_{\mathrm{r}}(p)}{C_{\mathrm{r}}(p)} = \frac{\left(K_{\mathrm{p}}\cdot p + K_{\mathrm{i}}\right)}{J\cdot p^2 + \left(K_{\mathrm{p}} + f\right)\cdot p + K_{\mathrm{i}}} = \frac{p\cdot\sigma + \omega_{\mathrm{n}}^2}{p^2 + 2\cdot\xi\cdot\omega_{\mathrm{n}} p + \omega_{\mathrm{n}}^2}$$

$$\hat{C}_{\mathrm{r}}(p) = G_1(p)\times\Theta_{\mathrm{ref}}(p) + G_2(p)\times C_{\mathrm{r}}(p)$$

On Figures 7.19 and 7.20 are presented the variations of the transfer functions between the observed torque and the reference position when the inertia and the friction are varied

7.4.3. *Complete order observer*

The development of this torque observer is based on the theory of state observers [BAB 91, LUE 71, VER 88]. There is, however, another approach based on the use of

a proportional integral regulator associated with a model. The observed torque is then given by this model's integrator output, as the input is the error between measured speed and its estimate [LEP 93].

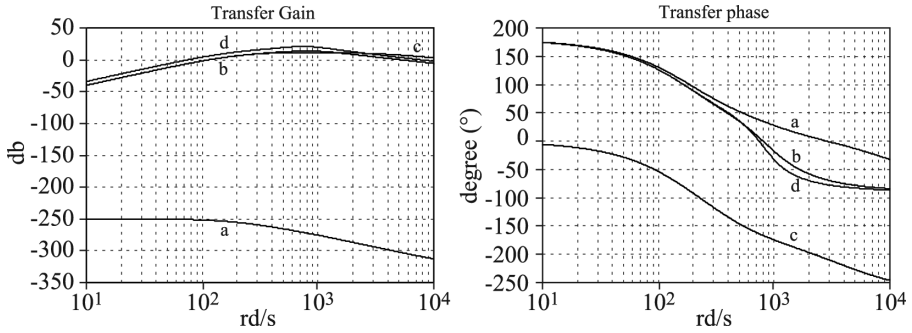

Figure 7.19. *Variation of inertia: Crobs transfer function in relation to θ_{ref} with (a) $J = J_n$; (b) $J = J_n + 50\%$; (c) $J = J_n - 50\%$; (d) $J = J_n + 100\%$*

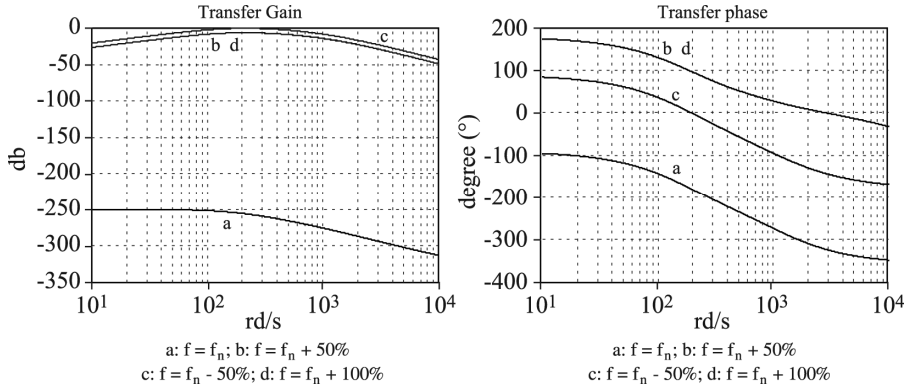

Figure 7.20. *Friction variation*

To apply this theory of state observers, in the case of the disruption torque, we consider the resistant torque as an additional state variable.

The hypothesis adopted by all publications consulted considers the resistant torque to be constant between two sampling moments [IWA 93, KO 93, REI 91]; this hypothesis is all the more justified as the sampling period is short:

$$C_r(k+1) = C_r(k)$$

With this additional state equation, the observer state model is:

$$\begin{pmatrix} \Omega(k+1) \\ \theta(k+1) \\ C_{\mathrm{r}}(k+1) \end{pmatrix} = \begin{bmatrix} F_{\mathrm{m11}} & 0 & H_{\mathrm{v1}} \\ F_{\mathrm{m21}} & 1 & H_{\mathrm{v2}} \\ 0 & 0 & 1 \end{bmatrix} \cdot \begin{pmatrix} \Omega(k) \\ \theta(k) \\ C_{\mathrm{r}}(k) \end{pmatrix} + \begin{bmatrix} H_{\mathrm{m1}} \\ H_{\mathrm{m2}} \\ 0 \end{bmatrix} \cdot I(k) \qquad [7.50]$$

In the following calculations, the observer parameters are taken as equal to the parameters of the actuator in order to avoid an excessive complexity of calculations.

It is then not possible to use the analytical study of transfer functions developed in this section to evaluate the influence of parametric variations on the actuator. This robustness study will be done later.

7.4.3.1. *Considerations on observability*

We will extend the study briefly presented in section 7.3.3, to an order three observer from the matrix of evolution [*F*], and output matrix [*C*].

This output matrix can take different forms, depending on whether the output variable is the position or speed. We then have:

$$[F] = \begin{bmatrix} F_{\mathrm{m11}} & 0 & H_{\mathrm{v1}} \\ F_{\mathrm{m21}} & 1 & H_{\mathrm{v2}} \\ 0 & 0 & 1 \end{bmatrix} \qquad [7.51]$$

If the position is output variable: [*C*] = [0 1 0]. The system can be observed if the following determinant is different from zero (application of the Kalman criterion):

$$\begin{vmatrix} [C] \\ [C]\cdot[F] \\ [C]\cdot[F]^2 \end{vmatrix} = \begin{vmatrix} 0 & 1 & 0 \\ F_{\mathrm{m21}} & 1 & H_{\mathrm{v2}} \\ F_{\mathrm{m21}}\cdot(1+F_{\mathrm{m11}}) & 1 & F_{\mathrm{m21}}\cdot H_{\mathrm{v1}} + 2\cdot H_{\mathrm{v2}} \end{vmatrix}$$

or

$$\begin{vmatrix} [C] \\ [C]\cdot[F] \\ [C]\cdot[F]^2 \end{vmatrix} = T\cdot\frac{J}{f^2}\cdot\left(1-\mathrm{e}^{-\frac{f}{J}T_{\mathrm{e}}}\right) \neq 0 \qquad [7.52]$$

The system can then be observed from the measure of position. Consequently, it is possible to reconstitute the disruption torque as well as the speed from the measure of position and knowledge of the current set point. Let us observe if this observability remains true in the case of the measure of speed only. The output matrix is then: $[C] = [1\ 0\ 0]$, and the determinant calculation defined previously is:

$$\begin{vmatrix} [C] \\ [C]\cdot[F] \\ [C]\cdot[F]^2 \end{vmatrix} = \begin{vmatrix} 1 & 0 & 0 \\ F_{\mathrm{m11}} & 0 & H_{\mathrm{v1}} \\ F_{\mathrm{m11}}^2 & 0 & H_{\mathrm{v1}}\cdot(1+F_{\mathrm{m11}}) \end{vmatrix} = 0 \qquad [7.53]$$

This determinant is zero and the system is therefore not observable from the measure of speed. As before (section 7.3.3), the initial position is not defined. We have here the same result as in [7.21] in the context of controllability and observability analysis for the development of modal control. According to [7.50], speed and torque do not depend on position. We can therefore delete the line involving the position in [7.50], and the reduced state system, without position, becomes:

$$\begin{pmatrix} \Omega(k+1) \\ C_{\mathrm{r}}(k+1) \end{pmatrix} = \underbrace{\begin{bmatrix} F_{\mathrm{m11}} & H_{\mathrm{v1}} \\ 0 & 1 \end{bmatrix}}_{F_{\mathrm{r}}} \cdot \begin{pmatrix} \Omega(k) \\ C_{\mathrm{r}}(k) \end{pmatrix} + \begin{bmatrix} H_{\mathrm{m1}} \\ 0 \end{bmatrix} \cdot I(k) \qquad [7.54]$$

$$\Omega(k) = \underbrace{[1 \quad 0]}_{C} \cdot \begin{pmatrix} \Omega(k) \\ C_{\mathrm{r}}(k) \end{pmatrix} \qquad [7.55]$$

The application of the Kalman criterion for the observability of the reduced system, with speed already measured is:

$$\begin{vmatrix} [C] \\ [C]\cdot[F_{\mathrm{r}}] \end{vmatrix} = \begin{vmatrix} 1 & 0 \\ F_{\mathrm{m11}} & H_{\mathrm{v1}} \end{vmatrix} = H_{\mathrm{v1}} = \frac{1}{f}\cdot\left(\mathrm{e}^{-(f/J)\cdot T_{\mathrm{e}}} - 1\right) \neq 0 \qquad [7.56]$$

The reduced state system [7.54, 7.55] is observable, and the knowledge of position is not necessary to estimate the resistant torque; the measure of speed is sufficient. In the mechanical equation, the speed and the sum of torques applied to the axis alone are involved. This speed measure does not make it possible to reconstitute the position because of the fact that the initial position is not known.

This order three observer estimates the state vector of components $\Omega(k), \theta(k)$, and $C_{\mathrm{r}}(k)$ from the current set point and measure of position, which is less noisy than the analog speed measure [KO 93]. It helps in setting up higher

observation dynamics, but we must have good resolution of the position encoder in order to protect against quantification noises.

7.4.3.2. *Construction*

From [7.50], the complete observer equation [7.57] is [KO 93]:

$$\begin{pmatrix} \widehat{\Omega}(k+1) \\ \hat{\theta}(k+1) \\ \hat{C}_{\mathrm{r}}(k+1) \end{pmatrix} = \begin{bmatrix} F_{\mathrm{m11}} & 0 & H_{\mathrm{v1}} \\ F_{\mathrm{m21}} & 1 & H_{\mathrm{v2}} \\ 0 & 0 & 1 \end{bmatrix} \cdot \begin{pmatrix} \widehat{\Omega}(k) \\ \hat{\theta}(k) \\ \hat{C}_{\mathrm{r}}(k) \end{pmatrix} + \begin{bmatrix} H_{\mathrm{m1}} \\ H_{\mathrm{m2}} \\ 0 \end{bmatrix} \cdot I(k) + \begin{bmatrix} l_1 \\ l_2 \\ l_3 \end{bmatrix} \cdot \left(\theta(k) - \begin{bmatrix} 0 & 1 & 0 \end{bmatrix} \cdot \begin{pmatrix} \widehat{\Omega}(k) \\ \hat{\theta}(k) \\ \hat{C}_{\mathrm{r}}(k) \end{pmatrix} \right) \quad [7.57]$$

State variables are estimates ($\hat{\Omega}, \hat{\theta}$ and $\hat{C}_{\mathrm{r}}$) and the observer convergence is ensured by the gap between the measured position and estimated position [VER 88]. This gap acts on every observer variable through gains l_1, l_2, and l_3. The structure of this observer is given in Figure 7.21.

Equation [7.57] can then be expressed in this way:

$$\begin{pmatrix} \widehat{\Omega}(k+1) \\ \hat{\theta}(k+1) \\ \hat{C}_{\mathrm{r}}(k+1) \end{pmatrix} = \underbrace{\begin{bmatrix} F_{\mathrm{m11}} & -l_1 & H_{\mathrm{v1}} \\ F_{\mathrm{m21}} & 1-l_2 & H_{\mathrm{v2}} \\ 0 & -l_3 & 1 \end{bmatrix}}_{F_{03}} \cdot \begin{pmatrix} \widehat{\Omega}(k) \\ \hat{\theta}(k) \\ \hat{C}_{\mathrm{r}}(k) \end{pmatrix} + \underbrace{\begin{bmatrix} H_{\mathrm{m1}} \\ H_{\mathrm{m2}} \\ 0 \end{bmatrix}}_{H_{\mathrm{m}}} \cdot I(k) + \begin{bmatrix} l_1 \\ l_2 \\ l_3 \end{bmatrix} \cdot \theta(k) \quad [7.58]$$

Factors l_1, l_2, and l_3 help in setting up the observation dynamic, because they are involved in matrix F_{03}. These gains are defined as state feedback gains for modal control pole placement. Characteristic polynomial $\Delta_{03}(z)$ is calculated (denominator of [7.66]), and its factors are identified with the polynomial factors imposed by the specifications.

$$\Delta_{03}(z) = \det\left[z \cdot 1 - F_{03} \right] \quad [7.59]$$

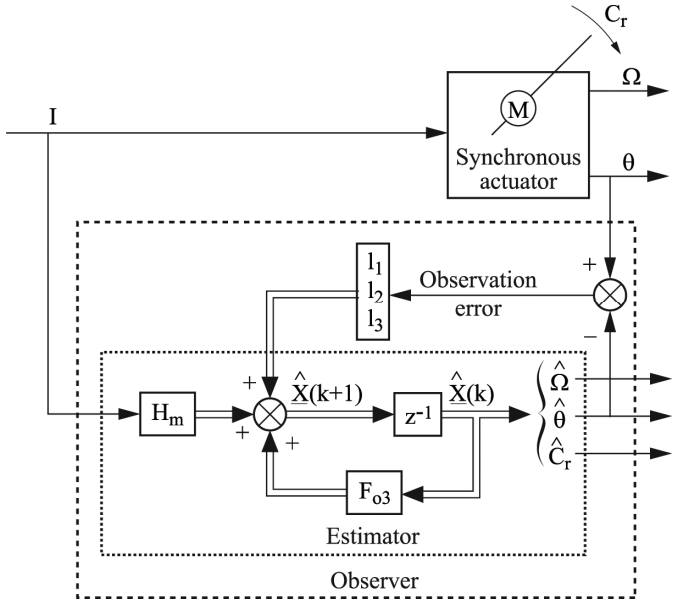

Figure 7.21. *Structure of the complete observer*

To impose three simple poles (p_1, p_2, and p_3), l_1, l_2, and l_3 must take values:

$$l_1 = \frac{H_{v1}\left(\left(1-p_1-p_2-p_3\right)\cdot\left(1+F_{m11}\right)+p_1\cdot p_2+p_2\cdot p_3+p_1\cdot p_3+F_{m11}^2\right)}{H_{v2}\cdot\left(1-\left(F_{m11}-F_{m21}\cdot\dfrac{H_{v1}}{H_{v2}}\right)\right)} + \frac{\left(p_1-F_{m11}\right)\cdot\left(p_2-F_{m11}\right)\cdot\left(p_3-F_{m11}\right)}{F_{m21}\cdot\left(1-\left(F_{m11}-F_{m21}\cdot\dfrac{H_{v1}}{H_{v2}}\right)\right)} \quad [7.60a]$$

$$l_2 = 2+F_{m11}-p_1-p_2-p_3 \quad [7.60b]$$

$$l_3 = \frac{\left(p_1-1\right)\cdot\left(p_2-1\right)\cdot\left(p_3-1\right)}{H_{v2}\cdot\left(\left(F_{m11}-F_{m21}\cdot\dfrac{H_{v1}}{H_{v2}}\right)-1\right)} \quad [7.60c]$$

By placing the three simple poles at the origin ($p_1 = p_2 = p_3 = 0$), the characteristic polynomial of the observer will be: $z^3 = 0$. We will then have an exact response observer that will reproduce the resistant torque with a delay of three sampling periods.

7.4.3.3. *Analytical study*

It is carried out with the constituted state equation of all equations corresponding to the actuator, observer, and control law. This global state equation of the closed-loop actuator provides transfer functions between state variables and input variables (reference position and load torque). The state equation of the motor is [7.15], that for the control law is given by [7.22] and [7.23], and that of the complete observer is [7.58]. State feedback in [7.23] is developed with observed variables $\hat{\Omega}(k)$ and $\hat{\theta}(k)$. Equation [7.23] is introduced in [7.15] and [7.58] and the global state equation is written as:

$$\underline{X}_{\text{glob}}(k+1) = F_{\text{glob}} \cdot \underline{X}_{\text{glob}}(k) + H_{\text{glob}} \cdot \begin{pmatrix} \theta_{\text{ref}}(k) \\ C_{\text{r}}(k) \end{pmatrix} \qquad [7.61]$$

with

$$\underline{X}_{\text{glob}}(k) = \begin{pmatrix} \Omega(k) \\ \theta(k) \\ X_{\text{r}}(k) \\ \hat{\Omega}(k) \\ \hat{\theta}(k) \\ \hat{C}_{\text{r}}(k) \end{pmatrix}$$

$$H_{\text{glob}} = \begin{bmatrix} H_{\text{m1}} \cdot K_{\theta} & H_{\text{v1}} \\ H_{\text{m2}} \cdot K_{\theta} & H_{\text{v2}} \\ 1 & 0 \\ H_{\text{m1}} \cdot K_{\theta} & 0 \\ H_{\text{m2}} \cdot K_{\theta} & 0 \\ 0 & 0 \end{bmatrix} \qquad [7.62]$$

$$F_{\text{glob}} = \begin{bmatrix} F_{\text{m11}} & 0 & H_{\text{m1}} \cdot K_{\text{r}} & -H_{\text{m1}} \cdot K_{\text{s1}} & -H_{\text{m1}} \cdot K_{\text{s2}} & H_{\text{m1}} \cdot K_{\text{v}} \\ F_{\text{m21}} & 1 & H_{\text{m2}} \cdot K_{\text{r}} & -H_{\text{m2}} \cdot K_{\text{s1}} & -H_{\text{m2}} \cdot K_{\text{s2}} & H_{\text{m2}} \cdot K_{\text{v}} \\ 0 & 0 & 1 & 0 & -1 & 0 \\ 0 & l_1 & H_{\text{m1}} \cdot K_{\text{r}} & F_{\text{m11}} - H_{\text{m1}} \cdot K_{\text{s1}} & -l_1 - H_{\text{m1}} \cdot K_{\text{s2}} & H_{\text{v1}} + H_{\text{m1}} \cdot K_{\text{v}} \\ 0 & l_2 & H_{\text{m2}} \cdot K_{\text{r}} & F_{\text{m21}} - H_{\text{m2}} \cdot K_{\text{s1}} & 1 - l_2 - H_{\text{m2}} \cdot K_{\text{s2}} & H_{\text{v2}} + H_{\text{m2}} \cdot K_{\text{v}} \\ 0 & l_3 & 0 & 0 & -l_3 & 1 \end{bmatrix} \quad [7.63]$$

The sixth column of F_{glob} is simplified with the help of relation [7.30], which defines compensation gain K_{v} of resistant torque. After simplification, this column is expressed according to:

$$^{t}\left(F_{\text{glob}}\left(\text{i},6\right)\right) = \left(-H_{\text{v1}} \quad -H_{\text{v2}} \quad 0 \quad 0 \quad 0 \quad 1\right) \quad [7.64]$$

Transfer functions provide the evolution of state variables of vector $\underline{X}_{\text{glob}}$ according to inputs θ_{ref} and C_{r}:

$$\underline{X}_{\text{glob}}\left(z\right) = \left[z \cdot 1 - F_{\text{glob}}\right]^{-1} \cdot H_{\text{glob}} \cdot \begin{pmatrix} \theta_{\text{ref}}(z) \\ C_{\text{r}}(z) \end{pmatrix} \quad [7.65]$$

This very large calculation was carried out with the help of the Mathematica software package [MTH 91]. The sixth line of $\underline{X}_{\text{glob}}$ [7.65] results in the observed torque according to system inputs. It depends only on the load torque and not on position set point. In the denominator in [7.66], the $\Delta_{03}\left(z\right)$ characteristic polynomial of the observer emerges, setting its dynamic from gains l_1, l_2, and l_3:

$$\hat{C}_{\text{r}}\left(z\right) = 0 \cdot \theta_{\text{ref}}\left(z\right) + \frac{l_3 \cdot H_{\text{v2}}\left(z - \left(F_{\text{m11}} - F_{\text{m21}} \cdot \dfrac{H_{\text{v1}}}{H_{\text{v2}}}\right)\right)}{\begin{pmatrix} F_{\text{m11}} \cdot \left(l_2 - 1 - l_3 \cdot H_{\text{v2}}\right) + F_{\text{m21}} \cdot \left(l_3 \cdot H_{\text{v1}} - l_1\right) \\ + z \cdot \left(1 + l_3 \cdot H_{\text{v2}} - l_2 + F_{\text{m21}} \cdot l_1 + 2 \cdot F_{\text{m11}} - F_{\text{m11}} \cdot l_2\right) \\ + z^2 \cdot \left(l_2 - F_{\text{m11}} - 2\right) \\ + z^3 \end{pmatrix}} \cdot C_{\text{r}}(z) \quad [7.66]$$

In a state of equilibrium, we can define that the observer's static gain equals 1, by applying the theorem of the final value in [7.66]. There is a zero at the numerator that depends only on mechanical parameters (J and f) and the sampling period:

$$Z_0 = F_{\text{m11}} - F_{\text{m21}} \cdot \frac{H_{\text{v1}}}{H_{\text{v2}}} = \frac{J \cdot \left(\lambda - 1\right) + \lambda \cdot f \cdot T_{\text{e}}}{J \cdot \left(\lambda - 1\right) + f \cdot T_{\text{e}}} \quad [7.67]$$

If the actuator is correctly identified, it is advantageous to compensate this zero with one of the poles of the observer characteristic polynomial in order to improve its dynamic behavior. The observer poles will then be: $p_1 = Z_0$, $p_2 = b$, and $p_3 = c$ and observer gains:

$$\left.\begin{aligned} l_1 &= \left(1 + F_{\text{m11}} - b - c\right) \cdot \frac{H_{\text{v1}}}{H_{\text{v2}}} \\ l_2 &= 2 + F_{\text{m21}} \cdot \frac{H_{\text{v1}}}{H_{\text{v2}}} - b - c \end{aligned}\right\} \Rightarrow l_1 = \left(l_2 - 1 + Z_0\right) \cdot \frac{H_{\text{v1}}}{H_{\text{v2}}}$$
$$l_3 = \frac{(b-1)\cdot(c-1)}{H_{\text{v2}}} \qquad [7.68]$$

If poles p_2 and p_3 are placed at the origin, the observer has an exact response in only two sampling periods. Compensation of Z_0 then accelerates the dynamic of the observer. Z_0 is between –1 and 0, causing alternation phenomena [BÜH 82] on the observation if the actuator parameters are not correctly identified, because Z_0 is no longer compensated. Through simulations, these alternation phenomena affect the inverter's control variable. From $\underline{X}_{\text{glob}}(z)$ in [7.65], the speed and position observation error can be defined. This error is the difference between real and observed state variables, components of $\underline{X}_{\text{glob}}(z)$:

$$\Omega(z) - \hat{\Omega}(z) = 0 \cdot \theta_{\text{ref}}(z) + \frac{(z-1)\cdot H_{\text{v1}} \cdot \left(z + l_2 - 1 - l_1 \cdot \dfrac{H_{\text{v2}}}{\text{H}_{\text{v1}}} \right)}{\Delta_{03}(z)} \cdot C_{\text{r}}(z) \qquad [7.69]$$

$$\theta(z) - \hat{\theta}(z) = 0 \cdot \theta_{\text{ref}}(z) + \frac{(z-1)\cdot H_{\text{v2}} \cdot (z - Z_0)}{\Delta_{03}(z)} \cdot C_{\text{r}}(z) \qquad [7.70]$$

The observation error is zero for variations of position set point but not for resistant torque variations. This error is canceled in a state of equilibrium because of term $(z-1)$ and the asymptotic convergence of the observer is ensured. Compensation of Z_0 by a $\Delta_{03}(z)$ pole decreases the effect of torque variations on the observation error [7.70], through the reduction of the transfer function sequence between the observation error and disruption torque. This compensation of Z_0 occurs also in [7.69] between l_1 and l_2 [7.68].

In summary, the resistant torque is estimated after two sampling periods in the case of zero compensation and the placement of a double pole at 0. In addition, the observation error of speed and position is not zero during load torque variations.

The complete theoretical structure, with performances that are not as good as the reduced structures discussed in the following text, was not implemented experimentally.

7.4.4. *Reduced order two observer based on the measure of position*

Since the error of observation is non-zero on position during load torque variations, and the measure of position is necessary for the complete observer, the measured position is used for the state feedback. In addition, for a zero or constant load torque, the observation error of the position is zero, regardless of the evolution of the position set point. The complete observer, therefore, has no advantage, not even a filtering effect to decrease the effects of quantification of the digital position encoder. In light of these comments, a reduced order two observer was developed for an observation of load torque and speed from current position and set point. It is a minimal Luenberger observer [BAB 91] where the measured variables are no longer being rebuilt.

7.4.4.1. *Construction*

Since position θ is measured, it is therefore no longer a state variable but an output variable of the reduced state system where the state variables observed are Ω and C_r.

Then, [7.50] is modified into:

$$\begin{pmatrix} \Omega(k+1) \\ C_r(k+1) \end{pmatrix} = \underbrace{\begin{bmatrix} F_{m11} & H_{v1} \\ 0 & 1 \end{bmatrix}}_{F_{r_r}} \cdot \begin{pmatrix} \Omega(k) \\ C_r(k) \end{pmatrix} + \begin{bmatrix} H_{m1} \\ 0 \end{bmatrix} \cdot I(k) \qquad [7.71]$$

$$\theta(k+1) - \theta(k) - H_{m2} \cdot I(k) = \begin{bmatrix} F_{m21} & H_{v2} \end{bmatrix} . \begin{pmatrix} \Omega(k) \\ C_r(k) \end{pmatrix}$$

This new state system is the basis of the reduced order two observer:

$$\begin{pmatrix} \hat{\Omega}(k+1) \\ \hat{C}_r(k+1) \end{pmatrix} = \begin{bmatrix} F_{m11} & H_{v1} \\ 0 & 1 \end{bmatrix} \cdot \begin{pmatrix} \hat{\Omega}(k) \\ \hat{C}_r(k) \end{pmatrix} + \begin{bmatrix} H_{m1} \\ 0 \end{bmatrix} \cdot I(k)$$
$$+ \begin{bmatrix} l_1 \\ l_2 \end{bmatrix} \cdot \left(\theta(k+1) - \theta(k) - H_{m2} \cdot I(k) = \begin{bmatrix} F_{m21} & H_{v2} \end{bmatrix} . \begin{pmatrix} \hat{\Omega}(k) \\ \hat{C}_r(k) \end{pmatrix} \right) \qquad [7.72]$$

As in [7.57], gains l_1 and l_2 ensure observer convergence from ratio [7.71] between the real actuator behavior and its observed behavior.

The structural diagram of this observer is shown in Figure 7.22. In equation [7.72], $\theta(k+1)$ at the second member is not known at moment k. In order to do this, we introduce variables $\hat{\Omega}'$ and $\hat{C}'_{\mathrm{r}}$ by the following transformation:

$$\begin{pmatrix} \hat{\Omega}(k+1) \\ \hat{C}_{\mathrm{r}}(k+1) \end{pmatrix} = \begin{pmatrix} \hat{\Omega}'(k+1) \\ \hat{C}'_{\mathrm{r}}(k+1) \end{pmatrix} + \begin{bmatrix} l_1 \\ l_2 \end{bmatrix} \cdot \theta(k+1) \qquad [7.73]$$

The reduced order two observer equation is:

$$\begin{aligned} \begin{pmatrix} \hat{\Omega}'(k+1) \\ \hat{C}'_{\mathrm{r}}(k+1) \end{pmatrix} &= \begin{bmatrix} F_{\mathrm{m11}} - l_1 \cdot F_{\mathrm{m21}} & H_{\mathrm{v1}} - l_1 \cdot H_{\mathrm{v2}} \\ -l_2 \cdot F_{\mathrm{m21}} & 1 - l_2 \cdot H_{\mathrm{v2}} \end{bmatrix} \cdot \begin{pmatrix} \hat{\Omega}'(k) \\ \hat{C}'_{\mathrm{r}}(k) \end{pmatrix} \\ &+ \begin{bmatrix} l_1 \cdot \left(F_{\mathrm{m11}} - l_1 . F_{\mathrm{m21}} - 1\right) + l_2 \cdot (H_{\mathrm{v1}} - l_1 \cdot H_{\mathrm{v2}}) \\ -l_2 \cdot \left(l_2 \cdot H_{\mathrm{v2}} + l_1 \cdot F_{\mathrm{m21}}\right) \end{bmatrix} \\ &+ \begin{bmatrix} H_{\mathrm{m1}} - l_1 \cdot H_{\mathrm{m2}} \\ -l_2 \cdot H_{\mathrm{m2}} \end{bmatrix} \cdot I(k) \end{aligned} \qquad [7.74]$$

The variables observed at moment k are deduced from transformation [7.73]. Gains l_1 and l_2, setting the observation dynamic, are determined by the identification of the characteristic polynomial of observer $\Delta_{02}(z)$ with the polynomial defined by the specifications:

$$\left(z - p_1\right) \cdot \left(z - p_2\right) = \Delta_{02}(z) = \begin{vmatrix} z - F_{\mathrm{m1}} + l_1 \cdot F_{\mathrm{m21}} & l_1 \cdot H_{\mathrm{v2}} - H_{\mathrm{v1}} \\ l_2 \cdot F_{\mathrm{m21}} & z - 1 + l_2 \cdot H_{\mathrm{v2}} \end{vmatrix} \qquad [7.75]$$

is explained in denominator [7.80]. For two simple poles (p_1 and p_2),

$$\begin{aligned} l_1 &= \frac{\left(p_1 + p_2\right) \cdot \left(H_{\mathrm{v2}} \cdot F_{\mathrm{m11}} - H_{\mathrm{v1}} \cdot F_{\mathrm{m21}}\right) - H_{\mathrm{v2}} \cdot \left(F_{\mathrm{m11}}^2 + p_1 \cdot p_2\right) + H_{\mathrm{v1}} \cdot F_{\mathrm{m21}} \left(1 + F_{\mathrm{m11}}\right)}{F_{\mathrm{m21}} \cdot \left(H_{\mathrm{v2}} \cdot \left(1 - F_{\mathrm{m11}}\right) + H_{\mathrm{v1}} \cdot F_{\mathrm{m21}}\right)} \\ l_2 &= \frac{\left(p_1 - 1\right) \cdot \left(p_2 - 1\right)}{H_{\mathrm{v2}} \cdot \left(1 - F_{\mathrm{m11}}\right) + H_{\mathrm{v1}} \cdot F_{\mathrm{m21}}} \end{aligned} \qquad [7.76]$$

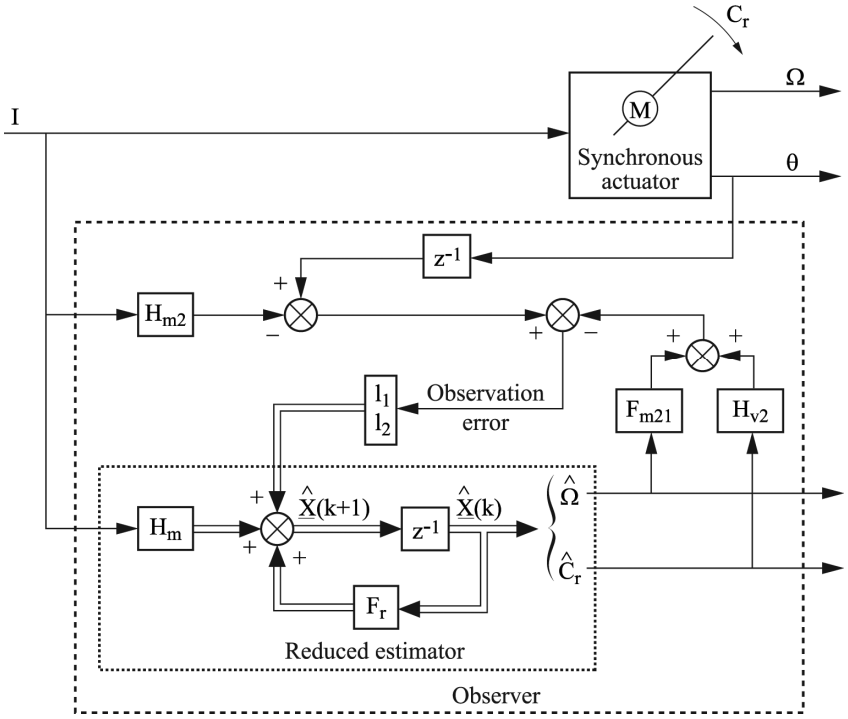

Figure 7.22. *Structure of the reduced order two observer*

7.4.4.2. *Analytical study*

This study is similar to the one carried out previously (section 7.4.3.3) and consists of combining state equations [7.15], those of control law [7.22, 7.23] and of observer [7.74] into a single equation. State equations of the observer involve $\hat{\Omega}$ and $\hat{C}_r'$ and control law, as observed speed is used for state feedback. The global state vector is:

$$\underline{X}_{glob}(k) =^{t} \left(\Omega(k) \quad \theta(k) \quad X_r(k) \quad \hat{\Omega}'(k) \quad \hat{C}_r'(k)\right) \qquad [7.77]$$

The variables observed are not components of $\underline{X}_{glob}(k)$, contrary to the complete observer.

Output matrix C_{glob}, deducted from [7.73], helps to determine the transfer functions:

$$\underline{y}(k) = \begin{pmatrix} \hat{\Omega}(k) \\ \hat{C}_{\text{r}}(k) \\ \Omega(k) \end{pmatrix} = \underbrace{\begin{bmatrix} 0 & l_1 & 0 & 1 & 0 \\ 0 & l_2 & 0 & 0 & 1 \\ 1 & 0 & 0 & 0 & 0 \end{bmatrix}}_{C_{\text{glob}}} \cdot \underline{X}_{\text{glob}}(k) \qquad [7.78]$$

The z transform of $y(k)$, expressed according to C_{glob}, F_{glob}, and H_{glob}, is linked to input variables by transfer functions.

$$\underline{y}(z) = C_{\text{glob}} \cdot \left[z \cdot 1 - F_{\text{glob}} \right]^{-1} \cdot H_{\text{glob}} \cdot \begin{pmatrix} \theta_{\text{ref}}(z) \\ C_{\text{r}}(z) \end{pmatrix} \qquad [7.79]$$

But matrices F_{glob} and H_{glob} have different factors than [7.62] and [7.63]. As before, this calculation was carried out with the help of the Mathematica software package. The second line of $\underline{y}(z)$ gives the expression of the observed torque expressed as:

$$\hat{C}_{\text{r}}(z) = 0 \cdot \theta_{\text{ref}}(z) + \frac{l_2 \cdot H_{\text{v2}} \left(z - \left(F_{\text{m11}} - F_{\text{m21}} \cdot \dfrac{H_{\text{v1}}}{H_{\text{v2}}} \right) \right)}{\begin{pmatrix} F_{\text{m11}} - F_{\text{m21}} \cdot l_1 - l_2 \left(F_{\text{m11}} \cdot H_{\text{v2}} - F_{\text{m21}} \cdot H_{\text{v1}} \right) \\ - z \cdot \left(1 + F_{\text{m11}} - F_{\text{m21}} \cdot l_1 - l_2 \cdot H_{v2} \right) \\ + z^2 \end{pmatrix}} \qquad [7.80]$$

As with the complete observer, the observed torque depends only on load torque, zero Z_0 at the numerator is the same, and static gain equals 1. If the zero is not compensated, the minimal observer response time will be of two sampling periods with an exact response if we put a double pole at the base. If mechanical parameters (J and f) are correctly identified, the compensation of Z_0 by one of the $\Delta_{02}(z)$ poles improves the behavior of the observer, because the transfer function between the load torque and its estimate is of the first order. If the second pole is placed at zero, the response is done in one sampling period. As before (section 7.4.3.3.), in the case of incorrect identification of the actuator, the zero is no longer compensated, and the observer consequently presents a negative pole that can cause an alternation of the observed torque. This alternation can then affect inverter control and be harmful to the actuator. To compensate the zero ($p_1 = Z_0$), observer gains are:

$$l_1 = \frac{H_{\text{v1}}}{H_{\text{v2}}} \quad \text{and} \quad l_2 = \frac{1 - p_2}{H_{\text{v2}}} \qquad [7.81]$$

The transfer function linking the observed torque to the disruption torque is:

$$\hat{C}_r(z) = 0 \cdot \theta_{ref}(z) + \frac{l_2 \cdot H_{v2}}{\left(z - \underbrace{\left(1 - l_2 \cdot H_{v2}\right)}_{p_2}\right)} \cdot C_r(z) \quad [7.82]$$

The observed torque is an image of the load torque seen through a filter of the first order of adjustable dynamics. From [7.79], the gap between the real speed and the observed speed is written as:

$$\Omega(z) - \hat{\Omega}(z) = 0 \cdot \theta_{ref} + \frac{(z-1)\left(H_{v1} - H_{v2} l_1\right)}{\Delta_{02}(z)} C_r(z) \quad [7.83]$$

The error on speed is zero regardless of the position reference but depends on load torque. Because of the term $(z - 1)$, it is canceled after a certain period of time when the load torque remains constant. The Z_0 compensation cancels the speed observation error even when the load torque varies, because the term $(H_{v1} - H_{v2} \cdot l_1)$ in [7.83] is canceled because of the l_1 sizing in [7.81]. If there is compensation of zero and simple pole placement at 0, the response of the reduced order two observer is of one sampling period. It also gives an unbiased image of speed, regardless of the load torque variations. The reduced order two observer offers better performances than the observer.

7.4.4.3. *Experimental tests*

The tests consist of maintaining the actuator position constant when its axis is disrupted by a load torque step. The behavior of the actuator with reduced order two observer is compared with or without torque compensation. The tests are done consecutively with a double pole and with a single pole by compensating the zero in the transfer function. The speed state feedback is done with observed speed. The dynamic of the state feedback is chosen slow enough, so that the modal control alone can present bad behavior in terms of disturbance rejection. The observer can then increase the dynamic of the disturbance rejection. The observation dynamic is higher than that of the state feedback because the compensation of the load torque occurs on the control variable.

We have not chosen an exact response, mentioned in the previous sections, of infinite observation dynamic ($p_{obs} = 0 \Rightarrow \omega_{obs} \to \infty$), because, as the measures are not

perfect, the noise considered by the observer would disrupt the operation of the actuator. The poles are chosen higher than 0.5 in a sample:

– *Choice of a double pole*: The parameters of the control law used for this test are as follows:

K_θ: compensation of pole $\omega_{bf} = 8$ rad/s;

$T_e = 5$ ms, $p_{obs} = p_1 = p_2 = 0.55 \Rightarrow \omega_{obs} \sim 120$ rad/s;

(double pole – behavior of the second order).

The observation error (Figure 7.22) depends on the measured position from a differentiating unit $(z-1)\cdot\theta(z)$. This measure of position must be exempt of any noise implying the implementation of a digital filter. The digital position encoder is less sensitive to disruptions than an analog encoder. The parasites in speed and torque analog measures (Figure 7.23) are more important than in the measure of position. However, digital encoding has quantification.

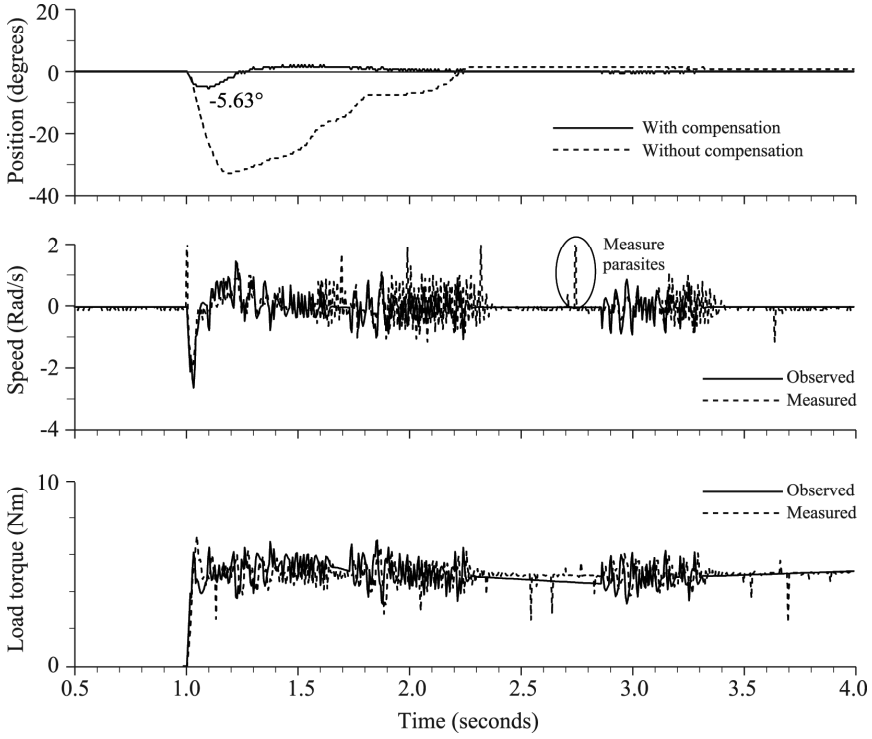

Figure 7.23. *Disturbance rejection behavior of reduced order two observer with double poles (experimental results)*

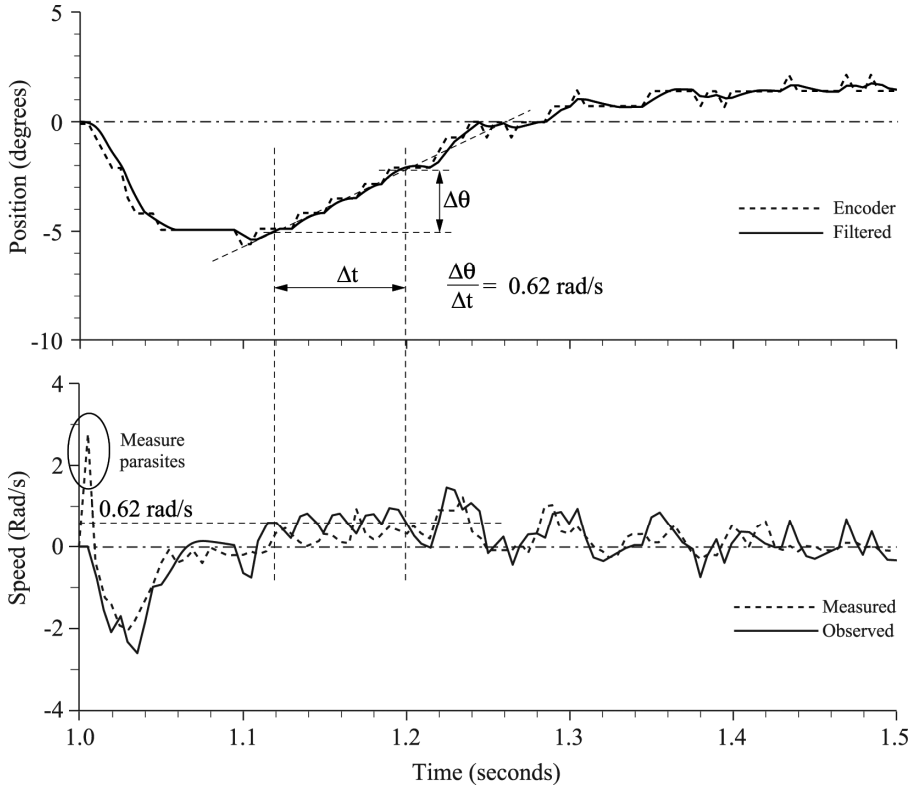

Figure 7.24. *Consideration of these effects of quantification of position encoder (experimental results)*

A too raw quantification, due to an insufficient resolution of the position encoder, results in quantification noise [MAR 65]. Here, the noise is not insignificant because the position is only encoded on 512 points per revolution (9 bits), or in other words, an encoder resolution of 0.7°. The measured position quantification (Figure 7.24) corresponds to disturbing steps, especially at slow speed. If this measure is injected as in the observer, the observed variables (torque and speed) show non-physical noises because of diversion.

A second-order digital filter reduces this quantification noise [SEV 82, MAX 88]. The characteristics of the equivalent continuous filter are:

– inherent angular frequency = 150 rad/s;

– damping factor = 0.61.

The inherent angular frequency of 150 rad/s minimizes phase shifting, caused by the filter at low frequencies. This filter provides a "smooth" image of the position measure (Figure 7.24) and decreases the harmful effects of quantification and results in a non-disrupted load torque and speed. In order to guarantee actuator stability, we must reduce dynamic performances of the control law because of the phase shift on the position caused by the filter. The sizing of this filter is the result of a compromise between the phase shift introduced and its ability to eliminate noises. The frequency of filter break is placed at least a decade beyond the control dynamic. The increase in the number of encoder bits decreases the quantification step and avoids the use of a filter. As an example, we can cite some publications that mention the use of 4,096-point (12 bit) encoders [CER 95], or with a larger number of points [MUR 93].

In Figure 7.23, the behavior of the actuator experiencing a torque step of 5 Nm (or ~ $0.5 \cdot C_{nom}$) is presented. The first gradient shows the influence of disruption rejection on the position; the position gap and response time are lower when the disruption torque is compensated.

The position without compensation (in dotted line) reveals the slot torque resulting in a rise in levels [MTS 93, VOR 96]. The two following reports (speed and load torque) correspond exclusively to the behavior of the actuator with compensation of load torque. The torque is not constant during transient mode, hindering the observation of speed [7.83]. These variations of torque are caused by the slot torque, function of position. In transient mode, a gap between measured torque and observed torque emerges and is linked to the effects of the filter on the measure of position and pole placement of the observer. In addition, the torque sensor has a second-order Butterworth filter with a bandwidth of 126 rad/s.

The observed torque has a slight sawtooth angular backlash around the measured torque when the position is not stabilized. It is caused by mechanical non-linearities, static friction torque, and dry friction torque [BRA 87]. This very low-frequency angular backlash is explained by the fact that the observed torque is built from the current set point, which is developed from torque observation. If the system was perfectly linear, an increase in the current set point would cause movement and the evolution of the observed torque. The position only varies when the motor torque exceeds a certain value because of static friction torque. An angular backlash of the position is then created around a steady state angle position. This limit cycle phenomenon is the subject of one of the experimental results presented later.

This angular backlash is made worse by the delay in detecting the variation of position because of the quantification of measure of position. It is visible at moments close to 3 s (Figure 7.23), and its amplitude is 0.7°, which is equal to the quantification step of the position encoder. The amplitude reduction of this angular

backlash is linked to a better encoder resolution. The speed observed (Figure 7.23) shows no parasites, contrary to the measured speed, which, with the suppression of the speed sensor, is a significant advantage. In Figure 7.24, there is a gap between the observed speed and the measured speed, during the torque step (between 1 and 1.1 s), caused by the phase shift of the filter on the measure of position, and on the other hand, by the error of observation of the observer. For very low speeds (<0.5 rad/s), the quality of speed observation decreases. This decrease has two reasons:

– The first reason is that at low speeds, the measure is tainted with errors caused by noises that are no longer insignificant on the low-weight bit of the analog digital speed converter (0.1 rad/s) (Figure 7.23 between moments 0.5 and 1 s).

– The second reason is linked to the effects of the quantification of the position measure and to those of the filter used to decrease it. During very slow movements (Figure 7.24), the speed observed is the derivative of the step response of this filter (between moments 1.34 and 1.37 s). The same applies to torque observation.

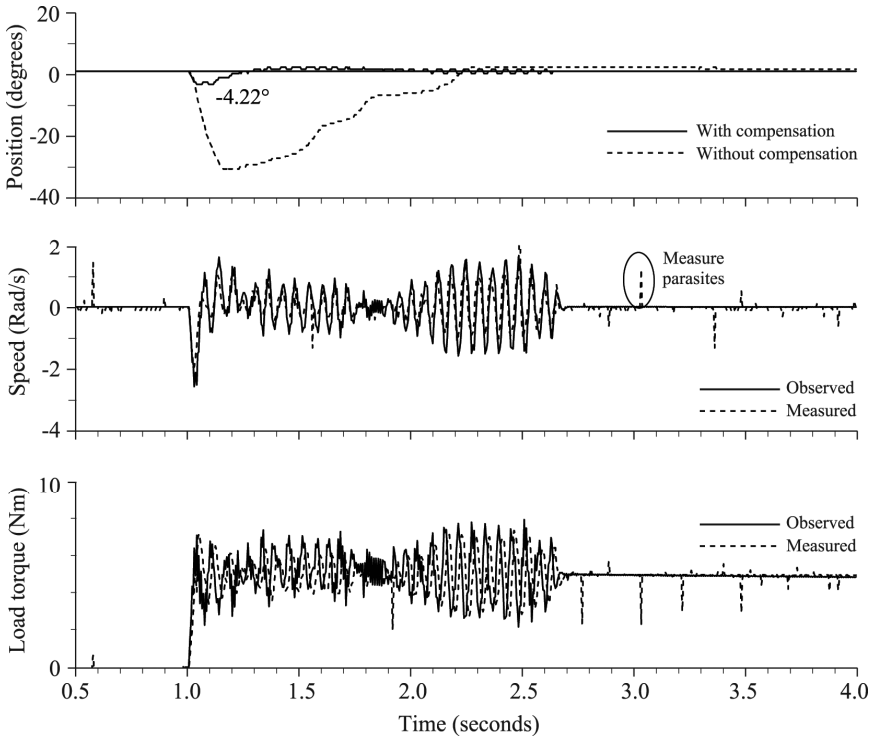

Figure 7.25. *Disturbance rejection behavior of reduced order two observer with single pole and zero compensation (experimental results)*

This filter is vital, however, except if a better-resolution position encoder is used. In Figure 7.25, the speed observed shows good correspondence in mean value with the real speed. Observed speed ripples are caused by quantification and the filter.

The quantification noise must be decreased by an appropriate filter so as not to destabilize the control law. This filtering deteriorates information, leading to a decrease in the performance of the control algorithm.

– *Choice of a single pole and zero compensation*: the control law and experimental tests (5 Nm torque step) are the same as in the previous case, but the observer pole is single: $p_{obs} = p_2 = 0.55 \Rightarrow \omega_{obs} \sim 120$ rad/s (single pole – first-order behavior).

The characteristics of the filter in the position measure are identical to the previous one (second-order cell with 150 rad/s angular frequency and damping factor 0.61). In Figure 7.25, the disturbance rejection behavior of the reduced order two observer with zero compensation is illustrated. We can verify better behavior; the position gap during the torque step is less than that without zero compensation (Figure 7.23). But the torque angular backlash (Figure 7.23) does not appear in Figure 7.25. The position and speed oscillations at the end of the transient mode (between 2 and 2.7 s) and similar in the test presented in Figure 7.23 are caused by the filters placed in the observed variables (torque and speed), introducing additional phase shifting. Since the observer with zero compensation is very sensitive to the quantification of the position encoder despite measure filtering, it is necessary to filter the observed variables, twice alternating the sampling period, such as observed speed (Figure 7.26). The observed speed (Figure 7.26) shows very low phase shift in relation to the speed measured, when zero is compensated [7.83]. The position quantification disrupts the observation, however, and requires filtering to be usable by modal control. This filtering introduces a phase shift liable to trigger the oscillations mentioned in the preceding text.

– *Conclusion*: in conclusion for these two tests, we can observe that the disturbance rejection is very efficient, compared with tests on the reduced order one observer (following section). These tests validate the use of observed speed for modal control and thus suppression of the speed sensor. The insufficient resolution of the position encoder does not make it possible to bring out all the possibilities of the observer. The quantification noise must be decreased by an appropriate filter so as not to destabilize control law. This filtering deteriorates information, leading to a decrease in the performance of the control algorithm.

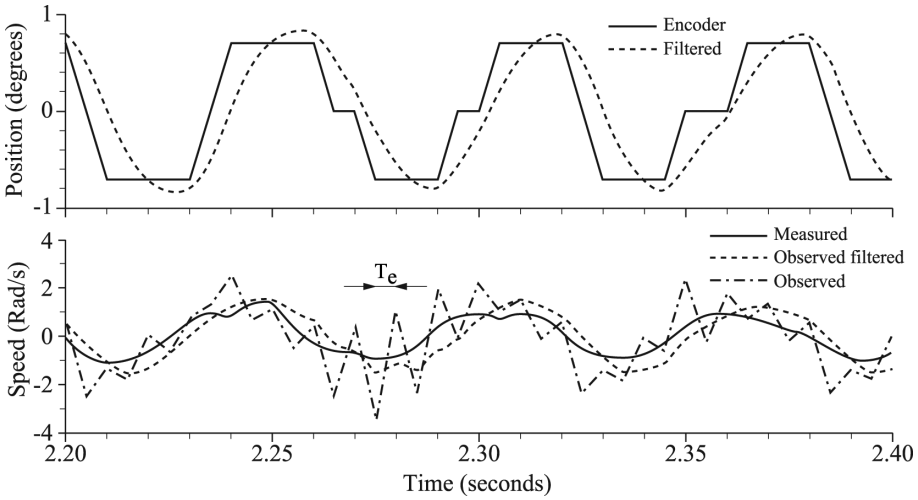

Figure 7.26. *Illustration of sensitivity to the quantification of reduced order two observer with zero compensation (experimental results)*

7.4.5. *Reduced order one observer based on speed measure*

It is possible (section 7.4.3) to observe the resistant torque only from the measure of speed. This justifies the study of the reduced order one observer to reconstitute the load torque from the measure of speed and current set point.

7.4.5.1. *Construction*

The construction of this observer is similar to that of reduced order two observer [7.54]. Since the speed is measured, it is no longer state variable but output variable. The state vector only has one component, the resistant torque, and observer output is a combination of the current set point and speed measured at different moments:

$$\begin{aligned} &C_{\mathrm{r}}\left(k+1\right)=C_{\mathrm{r}}(k)\\ &\Omega(k+1)-F_{\mathrm{m11}}\cdot\Omega(k)-H_{\mathrm{m1}}\cdot I(k)=H_{\mathrm{v1}}\cdot C_{\mathrm{r}}(k) \end{aligned} \qquad [7.84]$$

The observer equations are written as:

$$\begin{aligned} \hat{C}_{\mathrm{r}}\left(k+1\right) &= \hat{C}_{\mathrm{r}}\left(k\right)+l\cdot\left(\Omega\left(k+1\right)-F_{\mathrm{m11}}\cdot\Omega\left(k\right)-H_{\mathrm{m1}}\cdot I\left(k\right)-H_{\mathrm{v1}}\cdot\hat{C}_{\mathrm{r}}\left(k\right)\right)\\ &= \left(1-l\cdot H_{\mathrm{v1}}\right)\cdot\hat{C}_{\mathrm{r}}(k)+l\cdot\Omega(k+1)-l\cdot F_{\mathrm{m11}}\cdot\Omega\left(k\right)-l\cdot H_{\mathrm{m1}}\cdot I\left(k\right) \end{aligned} \qquad [7.85]$$

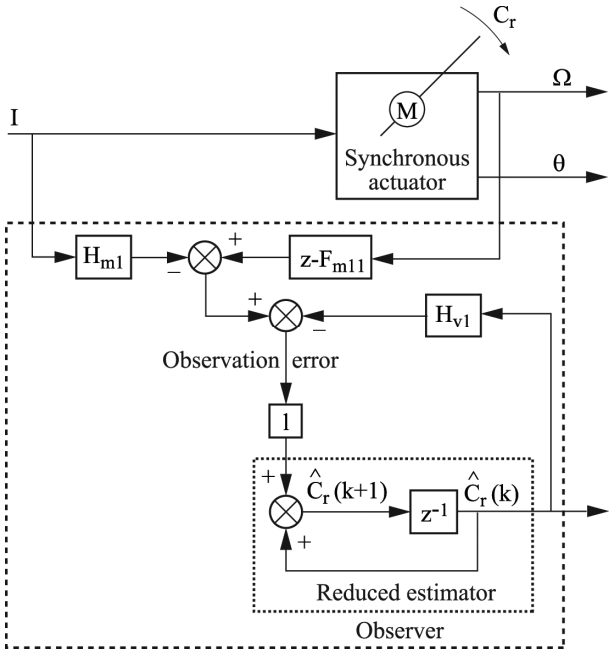

Figure 7.27. *Structure of the reduced order one observer*

The observer diagram is illustrated in Figure 7.27. Since $\Omega(k + 1)$ is not known at moment k, a change in variable is done:

$$\hat{C}_r(k+1) = \hat{C}'_r(k+1) + l \cdot \Omega(k+1) \quad [7.86]$$

Finally, the reduced order one observer has the following equations:

$$\begin{aligned} \hat{C}'_r(k+1) &= \underbrace{(1 - l \cdot H_{v1})}_{p_{obs}} \cdot \hat{C}'(k) + l \cdot (p_1 - F_{m11}) \cdot \Omega(k) - 1 \cdot H_{m1} \cdot I(k) \\ \hat{C}_r(k) &= \hat{C}'_r(k) + l \cdot \Omega(k) \end{aligned} \quad [7.87]$$

Gain l is sized from the choice of observation dynamic defined by p_{obs}:

$$l = \frac{1 - p_{obs}}{H_{v1}} \quad [7.88]$$

If $p_{obs} = 0$, we have an observer with exact response in one sampling period. The observation structure is very simple (Figure 7.28). Observer l gain is still negative because H_{v1} is negative and p_{obs} is between 0 and 1.

7.4.5.2. *Analytical study*

This study is similar to that done for the reduced order two observer, and the transfer function between the observed torque and inputs is:

$$\hat{C}_{\mathrm{r}}(z) = 0 \cdot \theta_{\mathrm{ref}}(z) + \frac{l \cdot H_{\mathrm{v1}}}{\left(z - \underbrace{(1 - l \cdot H_{\mathrm{v1}})}_{p_{\mathrm{obs}}} \right)} \cdot C_{\mathrm{r}}(z) \qquad [7.89]$$

The observed torque depends only on the load torque and the observer behaves as a first-order filter with a bandwidth that is set by gain *l*. This transfer function is comparable to the one defined in [7.82]. The reduced order one observer, therefore, has the same behavior as the reduced order two observer with zero compensation, but the latter also estimates the actuator speed without bias.

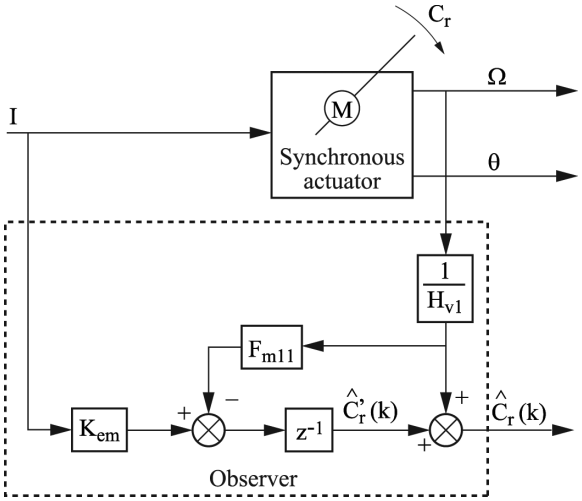

Figure 7.28. *Structure of the reduced order one exact response observer*

7.4.5.3. *Experimental results of the reduced order one observer*

As with reduced order two observer, we show here the role of the reduced order one observer in disturbance rejection. We compare the behavior of the actuator with or without load torque compensation.

The control law parameters in this test are determined as with the reduced order two observer (section 7.4.4.3):

– K_θ: compensation of pole, $\omega_{bf} = 8$ rad/s;

– $T_e = 5$ ms, $p_{obs} = 0.9 \Rightarrow \omega_{obs} \sim 21$ rad/s (first-order behavior).

Since the analog measure is noisy, it is necessary to filter it with a second-order digital filter [MAX 88]. The angular frequency inherent to the equivalent continuous filter equals 100 rad/s and its damping factor equals 0.6. This filter cannot completely support noises in speed measure. We must make sure that the filter does not introduce a phase shift in the speed measure, which would destabilize the control law. The torque sensor bandwidth is set at 126 rad/s by its second Butterworth filter (damping factor = 0.707). In Figure 7.29, the behavior of the actuator experiencing a torque step of 5 Nm or (~ $0.5 \cdot C_{nom}$) is illustrated.

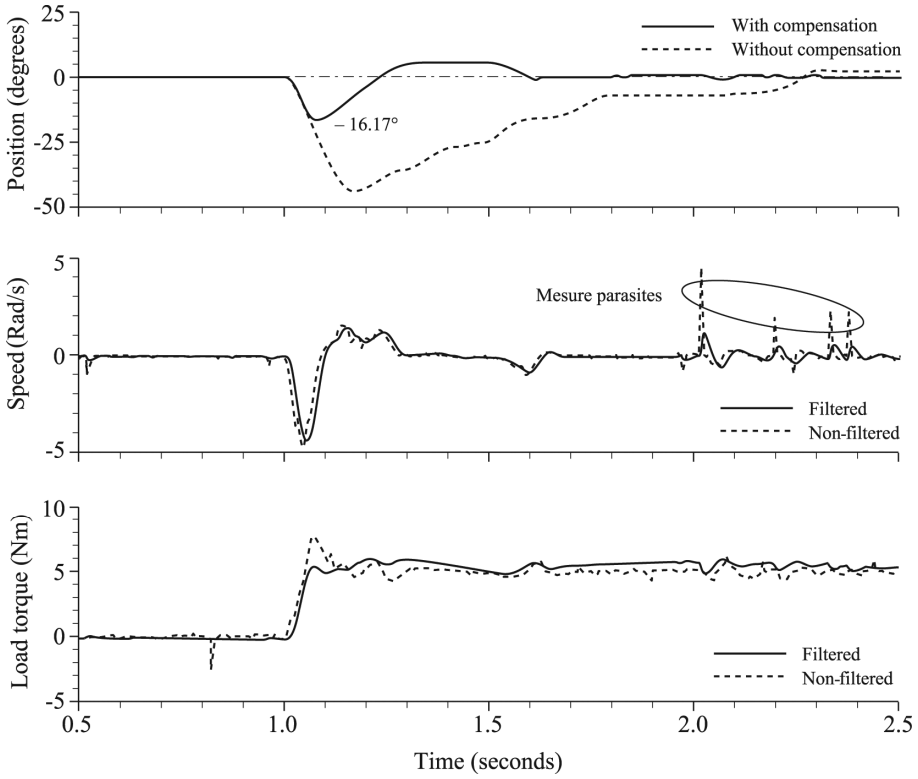

Figure 7.29. *Disturbance rejection behavior of reduced order one observer (experimental results)*

In the first gradient, the position gap and response time are lower when the load torque is compensated. As with the reduced order two observer, the slot torque results in a rise in levels in position without compensation (dotted line) [MTS 93, VOR 96]. But the reduced order two observer offers better rejection of the disturbance torque. The performances of the reduced order one observer had to be limited because of the speed measure noises. The two following gradients correspond to the actuator behavior with compensation of the load torque. Measured speed contains parasites that must be filtered without affecting the control law too much so it is not destabilized. The frequency of the filter break is placed at least a decade beyond the dynamic of state feedback, but the measure noises cannot be completely eliminated. Their effects are on the observed torque and position. The influence of these noises is minimized by reducing the control law and observer dynamics.

The difference between observed torque and measured torque is linked to this reduction of the observation dynamic. The measured torque peak is caused by the combined action of the slot torque (internal to the induction machine) and the effect of elasticity introduced by the torque sensor (installed between the two inertias). These phenomena result in ripples on the observed and measured torques (between t = 1 and 1.7 s). In a state of equilibrium (t = 1.9 s), the observed torque is higher than the measured torque, because of an incorrect identification of inverter gain or motor torque constant. If the observation error becomes too important, the behavior of the actuator then becomes disrupted (Figure 7.30).

The test (Figure 7.30) corresponds to a zero position set point and disturbance torque. The sensitivity of the observer to measure parasites (t = 0.17 s) and mechanical noise on the low-weight bit of the speed digital analog converter is brought out. The average non-zero filtered speed (between t = 0.22 and 0.45 s) triggers slow growth (in absolute value) of the observed torque and current set point to a threshold corresponding to the static friction torque. The position does not stabilize and shows oscillations caused by non-linear friction torques and the phase shift caused by speed filtering.

In conclusion, the presence of noises on the speed measure forces the reduction of control law performances. This is because of the filter in the speed measure on the one hand and the reduction of state feedback and observer dynamics on the other hand. The reduced order two observer enables the deletion of the speed sensor and gets rid of noise problems discussed previously.

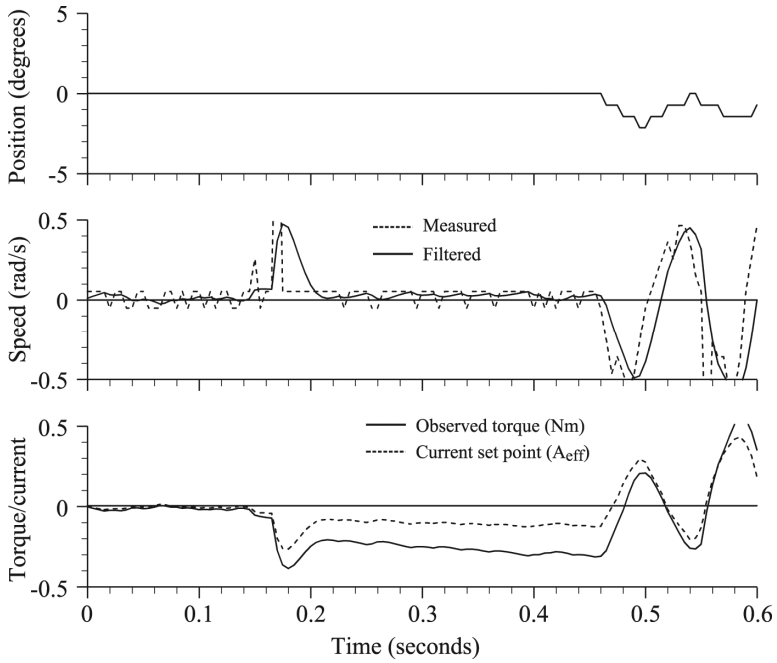

Figure 7.30. *Influence of noise on torque observation (experimental results)*

7.4.6. *Comparative study of different types of observers*

The different observation structures differ from the number of variables observed and the variable used to ensure observer convergence. Comparison Table 7.2 highlights the fact that the dynamic behavior of the observer depends on the number of variables observed. The observer response can be accelerated when zero is compensated by one of the poles and the observation dynamic is reduced by one order. In this way, reduced order two observer with zero compensated has the same dynamic behavior as the reduced order one observer and makes it possible to observe the speed without bias from the measure of position. This is only true with a good identification of mechanical parameters; otherwise, robustness of the control law is affected. The complete observer always has the worst dynamic. In this table, the noise problems linked to implementation do not appear.

The reduced order one observer requires the measure of speed, which is very sensitive to electromagnetic disturbances created by static converters that are hard to filter unless the measured speed is noticeably deteriorated by a significant phase shift. Since filtering does not eliminate all the noises, the dynamic of the order one observer must be reduced. This observer is, therefore, not an exact response, and a

compromise between the observation dynamic and influence of noises must be reached. If the measure of speed is very good, this structure, the simplest to implement, has the best response time (first-order dynamic), and the greatest robustness (see the following text).

		Complete observer	**Reduced order 2 observer**	**Reduced order 1 observer**
Measure used to ensure the observer convergence		θ	θ	Ω
Observed variables	$\hat{\theta}$	Yes	No	No
	$\hat{\Omega}$	Yes	Yes	No
	$\hat{C}_r$	Yes	Yes	Yes
Dynamic behavior of the observer		3rd order	2nd order	1st order
Presence of zero in the numerator of the transfer function		Yes	Yes	No
Dynamic behavior of the observer with zero compensation		2nd order	1st order	
Transient error of position observation	Without zero compensation	$\neq 0$	The position is not observed	
	With zero compensation	$\neq 0$		
Transient error of speed observation	Without zero compensation	$\neq 0$	$\neq 0$	The speed is not observed
	With zero compensation	$\neq 0$	$= 0$	

Table 7.2. *Comparison of the different observers*

With the reduced order two observer, based on the measure of position, the speed sensor and related problems are deleted. The digital position measure, which is less sensitive to electromagnetic disturbances, depends on the resolution of the encoder. If it is too low, a quantification noise filtering will be necessary, which may have a greater bandwidth and interfere less with the control law. In this way, the reduced order two observer bandwidth is greater and ensures better disturbance rejection than the reduced order one observer. The reduced order two observer has a second-order dynamic, therefore slower than the reduced order one observer, but it is

possible to make it faster with zero compensation. This zero compensation is very sensitive to the quantification of the measure of position (section 7.4.4.3) and requires good identification of parameters.

7.5. Robustness of control law by state feedback with observation of the resistant torque

7.5.1. *Introduction*

This part addresses the robustness of the control law when the actuator experiences parametric variations, that is, inertia, friction factor, and torque constant. The effect of these variations is quantified by the resulting position error and by the speed observation error when the observer evaluates the speed of the actuator. We first present the protocol of simulation used to evaluate robustness as well as the criterion of evaluation for position or speed errors. Then, we study the regulation robustness of the actuator through position error. For each parametric variation, the influence of the observation dynamic is evaluated. Finally, the influence of parametric variations on speed observation error is studied with the same approach as for the position error.

7.5.2. *Context of the study*

The protocol of the robustness study (Figure 7.31) is done on a machine with the characteristics indicated at the end of the chapter:

– a position step of 90° at no load;

– then a load torque step of 5 Nm (approximately half of the nominal torque) applied to the actuator.

Speed and position sensors are presumed to be perfect. In Figure 7.31, the real position, its set point, the real load torque, and that given by the reduced order one observer are represented:

$$\left(p_{\text{obs}} = 0.7 \quad \text{and} \quad \theta_{\text{obs}} \cong 18\,\text{rad/s}\right)$$

The characteristics of control law are:

$T_{\text{e}} = 20$ ms, $\theta_{\text{bf}} = 15$ rad/s, K_{θ}: zero compensation

The criterion of evaluation for position and speed errors is the integral of its absolute value:

$$\text{IAE} = \int \left|\text{error}(t)\right| \cdot \text{d}t \quad \text{with} \quad \begin{aligned} \text{error}(t) &= \theta_{\text{ref}}(t) - \theta(t) \\ \text{error}(t) &= \Omega(t) - \hat{\Omega}(t) \end{aligned} \qquad [7.90]$$

In the case of the position error, the *Integral Absolute Error* criterion (Figure 7.31) represents the surface (rad/s) between the position and its set point. In the case of the speed observation error, the unit is the radian.

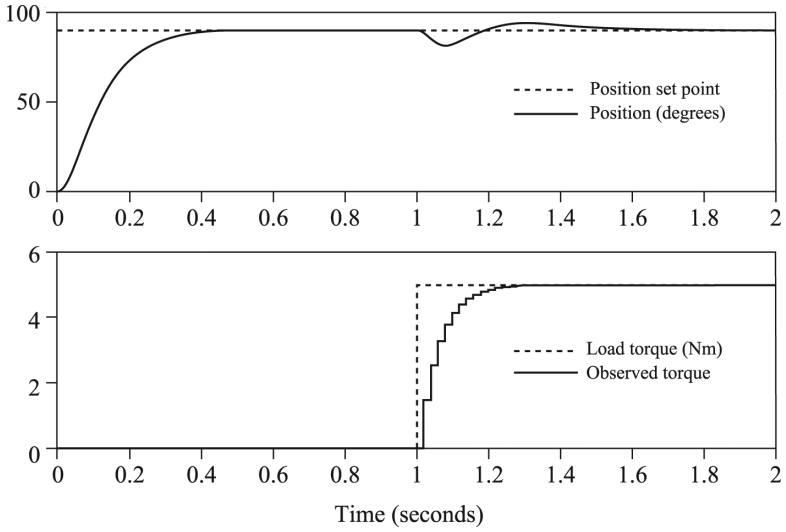

Figure 7.31. *Simulation profile*

Simulation results are presented in the form of graphics. For a parametric variation (moment of inertia, friction factor, or torque constant), we compare the error obtained with the following control laws:

– (*reso*) state feedback without observer;

– (*o1*) state feedback with torque compensation by the reduced order one observer;

– (*o2cz*) state feedback with speed observation and torque compensation by the reduced order two observer with zero compensation;

– (*o2p2*) state feedback with speed observation and torque compensation by double pole reduced order two observer;

– (*o3cz*) state feedback with position and speed observation, and torque compensation by complete observer with zero compensation;

– (*o3p3*) state feedback with position and speed observation, and torque compensation by triple pole complete observer.

The simulations are done with two observation dynamics:

– $p_{obs} = 0$ (deadbeat response observer);

– $p_{obs} = 0.7$ ($\omega_{obs} \sim 18$ rad/s).

In the reduced order two observer and complete observer, the state feedback is built with observed state variables (speed and position), knowing that the position observation is only available with the complete observer. The unstable cases are not represented in the graphics. The parametric variations (inertia, friction factor, and torque constant) are represented in the following way:

$$J = k \times J_n \quad \text{with} \quad k \in [0.5;1;2]$$
$$f = k \times f_n \quad \text{with} \quad k \in [0.1;0.5;1;2;10]$$
$$k_{em} = k \times (K_{em})_n \quad \text{with} \quad k \in [0.5;0.75;1]$$

7.5.3. *Robustness of actuator position*

We present here the robustness simulation results of the regulation actuator during the application of a torque step. We study the influence of the variations of inertia, friction factor, and torque constant for two observer dynamics.

7.5.3.1. *Variations of inertia*

The variations of inertia considered correspond to a doubling and a division by two of nominal inertia. The results are presented in Figure 7.32.

Robustness deteriorates with a quick observation dynamic and when the inertia decreases. In this case, the actuator becomes unstable with an observation structure.

To determine the control algorithm, it is therefore better to underestimate inertia if it is likely to change.

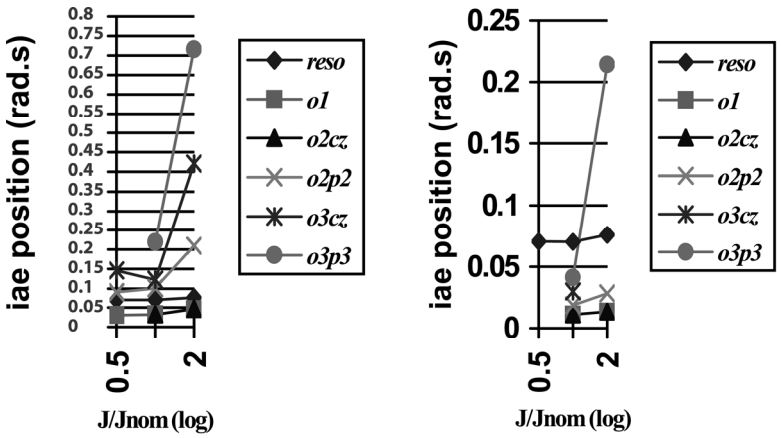

Figure 7.32. *Regulation robustness when inertia changes with (a) $p_{obs} = 0.7$ and (b) $p_{obs} = 0$*

When inertia increases, and with a quick observation dynamic, complete observers ((*o3cz*) and (*o3p3*)) are not robust, they can even be unstable.

For a slower observation dynamic, the risks of instability decrease but the position error caused by the torque step is, in certain cases, greater than the error obtained without the addition of the observation structure ((*o3p3*), (*o3cz*), and (*o2p2*)).

Here, only structures (*o1*) and (*o2cz*) remain competitive. In addition, structure (*o1*) remains stable when inertia decreases, which is not the case with structure (*o2cz*).

7.5.3.2. *Friction factor variations*

Robustness results are presented in Figure 7.33. It is affected very little by a decrease in friction factor, and overestimating the friction factor thus retains its advantage. As before, the observation structures with zero compensation ((*o2cz*) and (*o3cz*)) have increased instability risks. They are less significant, however, when the dynamic of observation is slow, but the disturbance rejection is less efficient.

In the case of structures (*o3p3*), (*o3cz*), and (*o2p2*), the disruption rejection error is even more significant than that without load torque compensation (*reso*). High observation structures do not have as good robustness as reduced structures. This is particularly visible in the case where $p_{obs} = 0.7$.

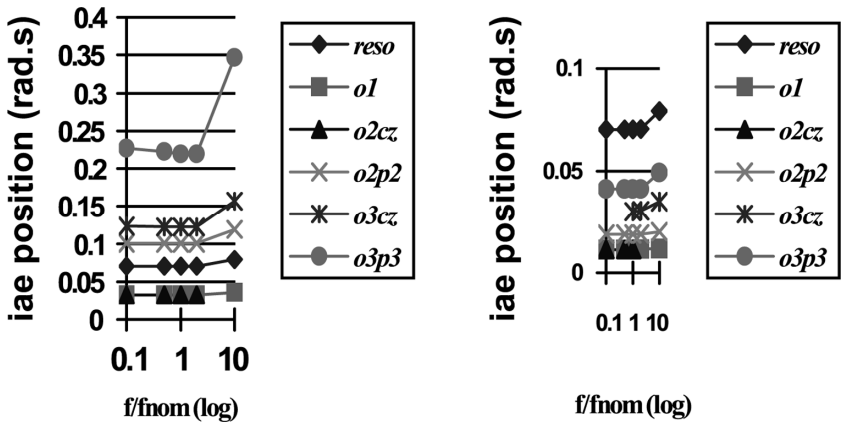

Figure 7.33. *Regulation robustness when the friction factor changes with (a)* $p_{obs} = 0.7$ *and (b)* $p_{obs} = 0$

In addition, structures (*o1*) and (*o2cz*) offer the same error when they are stable. Reduced order two and one observers with zero compensation [7.82, 7.89] behave as first-order systems for the observation of the resistant torque.

Observation dynamic being equal, the behavior is identical. Risks of structure (*o2cz*) instability can be attributed to the observation of speed in addition to the observation of the torque.

7.5.3.3. *Torque constant variations* (Figure 7.34)

Since these two observed variables are used by the control law, the actuator is more sensitive to parametric variations than with structure (*o1*), only giving torque observation.

The positioning error is almost doubled when the torque constant is divided by 2. For a quick observation dynamic, observation structures based on the complete observer are not robust or unstable ((*o3p3*) and (*o3cz*)).

The other structures provide good compensation of the torque step; but for a given structure, the variation of error remains relatively significant.

For slow observation dynamic, all the structures remain stable, but structures based on the complete observer and structure (*o2p2*) result in a more important regulation error than control law without torque compensation.

7.5.4. *Robustness of actuator rotation speed*

As before, this study is based on the use of criterion IAE applied at speed observation error, for observation structures also resulting in observed speed in addition to observed load torque ((*o2cz*), (*o2p2*), (*o3cz*), and (*o3p3*)).

We focus on regulation robustness, and on the influence of each parameter (moment of inertia, friction factor, and torque constant), for two observation dynamics.

7.5.4.1. *Variations of inertia*

Complete observation structures are not robust, a phenomenon that is more obvious as the observation dynamics are slow.

For quick observation dynamics, the speed observation error is less, but robustness is damaged.

The use of structure (*o2p2*), because of the relatively low observation error, seems to be the best solution as long as we choose an appropriate observation dynamic: a dynamic that is too quick makes this structure unstable when the inertia decreases (Figure 7.35).

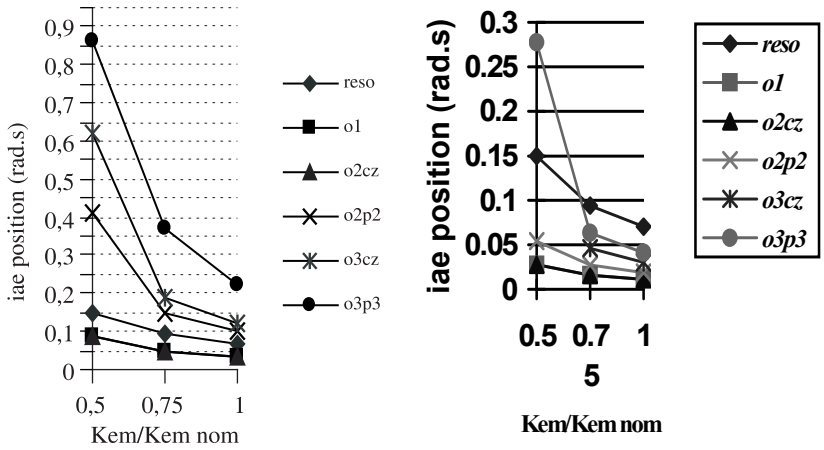

Figure 7.34. *Regulation robustness when torque constant changes with (a) $p_{obs} = 0.7$ and (b) $p_{obs} = 0$*

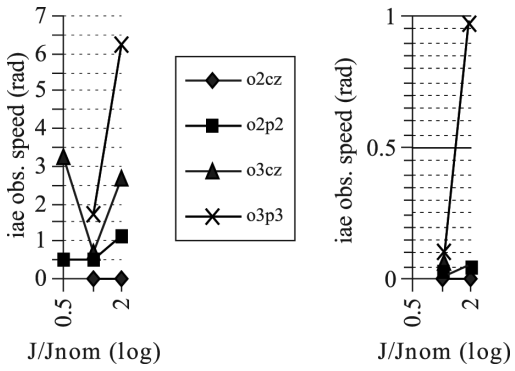

Figure 7.35. *Speed observation error in regulation when inertia changes with (a) $p_{obs} = 0.7$ and (b) $p_{obs} = 0$*

7.5.4.2. *Friction factor variations*

As in previous cases, it appears that the speed observation error is more significant when the observation dynamic is slow. This comment must be nuanced in the case of structure (*o2cz*), which can maintain a low observation error, even if the observation dynamic is slow. A quick observation dynamic decreases observation error, but zero compensation structures ((*o2cz*) and (*o3cz*)) can become unstable depending on the evolution of the friction factor. Structure (*o2p2*), with a quick observation dynamic, then seems to be a good compromise between robustness and precision when friction factor varies. This structure remains stable regardless of the variation of the friction factor. As in the previous cases, the complete structures are the weaker ones. Figure 7.36 illustrates these results.

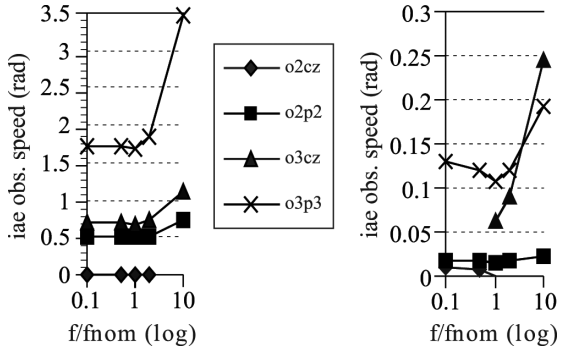

Figure 7.36. *Speed observation error in regulation when friction factor changes with (a) $p = 0.7$ and (b) $p_{obs} = 0$*

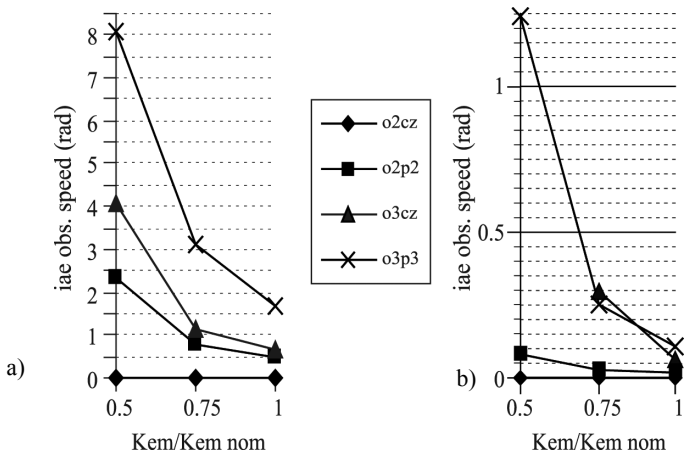

Figure 7.37. *Speed observation error in regulation with (a) $p_{obs} = 0.7$ and (b) $p_{obs} = 0$*

7.5.4.3. *Torque constant variations*

In regulation and tracking, the observation of speed by structure (*o2cz*) is completely insensitive to the variations of torque constant (Figure 7.37).

Complete structures also present an observation error quickly increasing when torque constant decreases. This error is all the more important as the observation dynamic is slow.

7.5.5. *Conclusions*

The results of simulations done previously are summarized in Table 7.3.

This table shows that the complete observer is the least advantageous. Its performances compared with reduced observers are globally worse in position error and speed observation as well as robustness.

If we have a speed sensor, the reduced order one observer has the best performance in terms of positioning error and robustness to parametric variations. This structure, contrary to the others, maintains a certain level of robustness when inertia decreases, as long as we do not use an observation dynamic that is too high. But the chain of speed measure must be exempt from any disturbance (section 7.4).

		(o1)	*(o2cz)*	*(o2p2)*	*(o3cz)*	*(o3p3)*
$p_{obs} = 0$	J ↗	**R**	**R**	**R**	**I**	**E**
	J ↘	**I**	**I**	**I**	**I**	**I**
	f ↗	**R**	**I**	**R**	**R**	**R**
	f ↘	**R**	**R**	**R**	**I**	**E**
	K_{em} ↘	**R**	**R**	**R**	**I**	**E**
	K_{em} ↗	**I**	**I**	**I**	**I**	**I**
$p_{obs} = 0{,}7$	J ↗	**R**	**R**	**E**	**E**	**E**
	J ↘	**R**	**I**	**E**	**E**	**I**
	f ↗	**R**	**I**	**E**	**E**	**E**
	f ↘	**R**	**R**	**E**	**E**	**E**
	K_{em} ↘	**R**	**R**	**E**	**E**	**E**
	K_{em} ↗	**I**	**I**	**I**	**I**	**I**

I: the actuator is unstable
E: the actuator remains stable, but the error of position is more significant than without the use of observation structure (*reso*)
R: the observation structure improves actuator robustness. The error of position is reduced in relation to control without observer (*reso*)

Table 7.3. *Comparison of robustness for parametric variations with different observation structures and according to the observation dynamic*

If we have a position sensor, the reduced order two observer has the advantage of being able to observe the disruption torque and speed from the measure of position only. There are two methods of placing the poles of this observer, which give a zero to the numerator. The first one (*o2cz*) consists of compensating zero by a pole and has similar performance as with the reduced order one observer but is more sensitive to variations of inertia and friction factor.

This drawback disappears by applying the second method (*o2p2*), consisting of placing a double pole (preferably at the origin), instead of compensating the zero. The control law is then more robust but its performances turn out to be lower in terms of torque rejection.

For the observer dynamic, the placement of p_{obs} at zero offers the best performance in disturbance rejection but has increased instability risks during parametric variations. These risks are lessened with a slower observation dynamic, by placing p_{obs} in 0.7, for example. In this case, the disturbance rejection is less efficient and robustness is not guaranteed for order two and three structures. It is then necessary to choose an appropriate observation dynamic (not too slow and not too quick), which does not make the actuator unstable, while maintaining good robustness during parametric variations.

Additional simulations have shown that this compromise is easier to find when the sampling period is shorter. The use of structure (*o2p2*) can then be interesting because it remains stable when inertia decreases and observation dynamic is not too quick. It must nevertheless be quick enough to maintain a good level of robustness.

The study carried out for reduced order one and two observers also shows that it is better to underestimate inertia and overestimate the friction factor during gains calculation of the control law; it enables us to be more efficiently protected against risks of instability linked to the variations of these two parameters. These risks are sensitive when the real mechanical time constant (J/f) is lower than the time constant used to determine control law. We must not underestimate the electromagnetic constant, however, because its increase in relation to the value used to size the control law makes the actuator unstable.

7.6. Experimental results

7.6.1. *Introduction*

To conclude this chapter, we present a few experimental results obtained in a benchmark (Figure 7.38). These results illustrate the behavior of the actuator according to the implemented control law.

We first study control law behavior by state feedback associated with a resistant torque observer, with mass hoisting tests involving parametric variations, and tests illustrating non-linear friction phenomena.

The actuator is made up of a self-guided synchronous machine powered by a soft switching PWM inverter, coupled with a direct current machine powered by a four-quadrant clipper configured as current source, resulting in a variable torque generator.

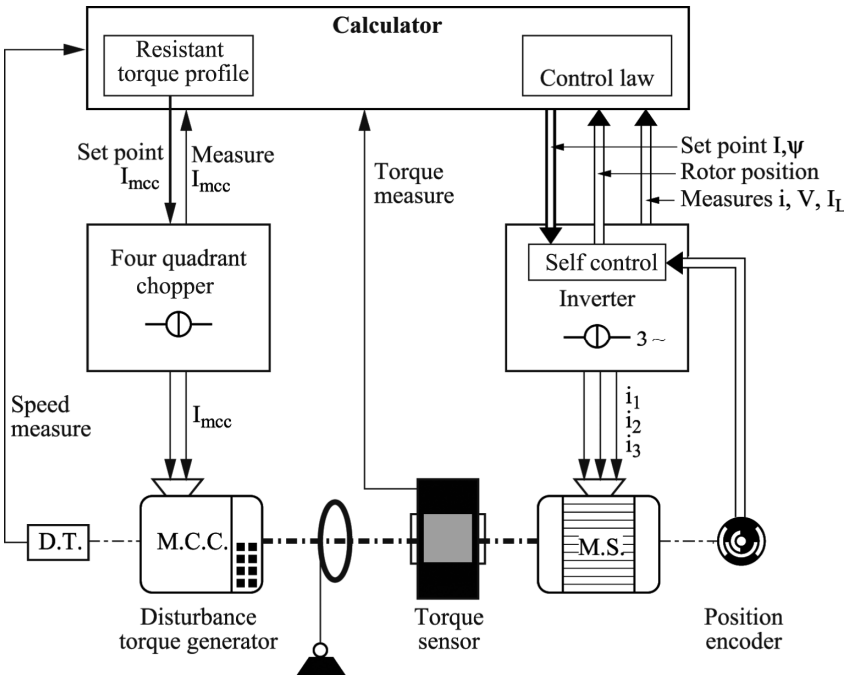

Figure 7.38. *Overview diagram of the experimental platform*

The bench is also equipped with a pulley (r = 44 mm) associated with a crane to enable mass hoisting operations that can reach 20 kg. A torque sensor, a tachometer generator, and absolute digital position encoder are coupled to machines.

A calculator monitors the operation in real time. It controls the position of the synchronous actuator and calculation of the current set point dedicated to the variable torque generator.

A photograph of the test platform is shown in Figure 7.39.

7.6.2. *Results of modal control with resistant torque observer*

All the tests were obtained with the reduced order two observer with double pole, based on a measure of position (section 7.4.5). This structure makes it possible to observe speed, used for state feedback, and results in greater robustness than the reduced order two structure with zero compensation (section 7.5).

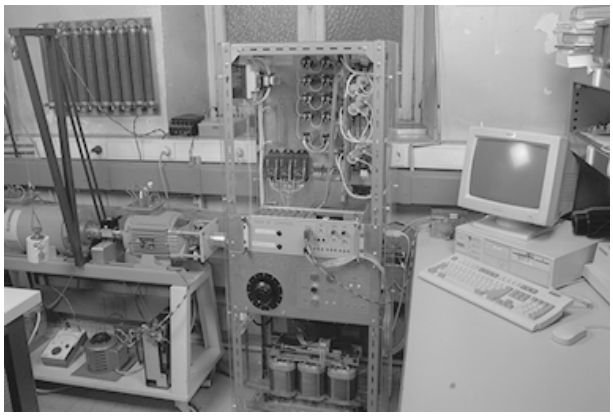

Figure 7.39. *Overview of the experimental platform*

Complete observation structures were not implemented because they showed worse performances than reduced structures (sections 7.4 and 7.5). Experimental results of the reduced order one structure were the subject of publications [VOR 95, VOR 96]. The tests were done with a 5 ms sampling period, or a sampling frequency of 200 Hz. The position is filtered by a second order digital filter with angular frequency of 150 rad/s and damping factor of 0.61. This filter lessens the effects of position measure quantification [MAX 88, SEV 82]. The direct intervention factor of set point K_θ is chosen to compensate a closed-loop pole and thus avoid overshoots. We then have a triple pole (section 7.3.4.2).

Observer poles were not placed at zero, and the observer is, therefore, not exact response, contrary to what theoretical developments recommended for a good restitution of the load torque (section 7.4.5). This observation dynamic reduction is due to insufficient resolution of the position encoder, as it creates problems of quantification (section 7.4.5.3), resulting in measuring noises, too disruptive for the observer if it has the exact response. The pole placement of the observer then depends on an acceptable noise level in the observation procedure. Despite this practical restriction, the results presented show good observer behavior. In the robustness study (section 7.5.5), the risks of actuator instability, for parametric variations, are reduced for a dynamic that is too quick.

7.6.2.1. *Mass lifting*

These tests consist of quickly elevating a 20-kg mass with the help of a pulley and crane (Figure 7.38), and then very slowly depositing it to show the disrupting effects of the slot torque of the synchronous machine. The load torque corresponding to this mass is approximately 8.6 Nm, since the pulley radius equals

44 mm. This 20-kg mass corresponds to a radial force of 196 N soliciting group steps.

The dynamics chosen for state feedback and observer correspond to:

$$\omega_{bf} = 3 \text{ rad/s}, p_{obs} = p_1 = p_2 = 0.7 \Rightarrow \omega_{obs} \sim 71 \text{ rad/s} \quad \text{(double pole)}$$

The dynamic of state feedback is placed at a very low value in order to show the addition of the observer in terms of load torque compensation. We compare two tests:

- the first one is done without load torque compensation ($K_v = 0$);
- the second one is done with load torque compensation ($K_v = 1/ (K_{em})_n$).

In both cases, the speed observed is used for state feedback. Figure 7.40 shows the advantage of compensating the disturbance torque, because the position with compensation is much closer than the position without compensation. State feedback control without compensation requires more time to hoist the mass.

During the descending phase, control without compensation is penalized by the cogging torque blocking the rotor in preferential positions in relation to the stator, blocking phenomenon heightened by stiction and static friction. These phenomena are not insignificant because of the radial force applied to the steps of the machine when the mass is suspended. The cogging torque is visible during the descending phase with compensation, by the small ripples on the position every 10° (spatial period of the cogging torque) (section 7.2.2.2). This last statement is illustrated in Figure 7.41 showing the torque observed according to position.

The tracking error, approximately 13.4° with torque compensation, reflects the theoretical predictions [7.39], resulting in an error of 13.7° with the control law parameters:

$$b = 0.349 \text{ rad/s}; \; K_{s2} = 0.3504; \; K_r = 0.0017; \; K_\theta = 0.1171$$

The torque observed is "parasited" when the position moves (Figure 7.40) because of the harmful effects of quantification on position measure (section 7.4.5.3). During the descending phase, the torque observed is lower than the torque created by the mass because of dry friction facing the movement created by the mass. The braking torque, generated by the motor, is thus lower than torque created by the mass, which explains the observation gap.

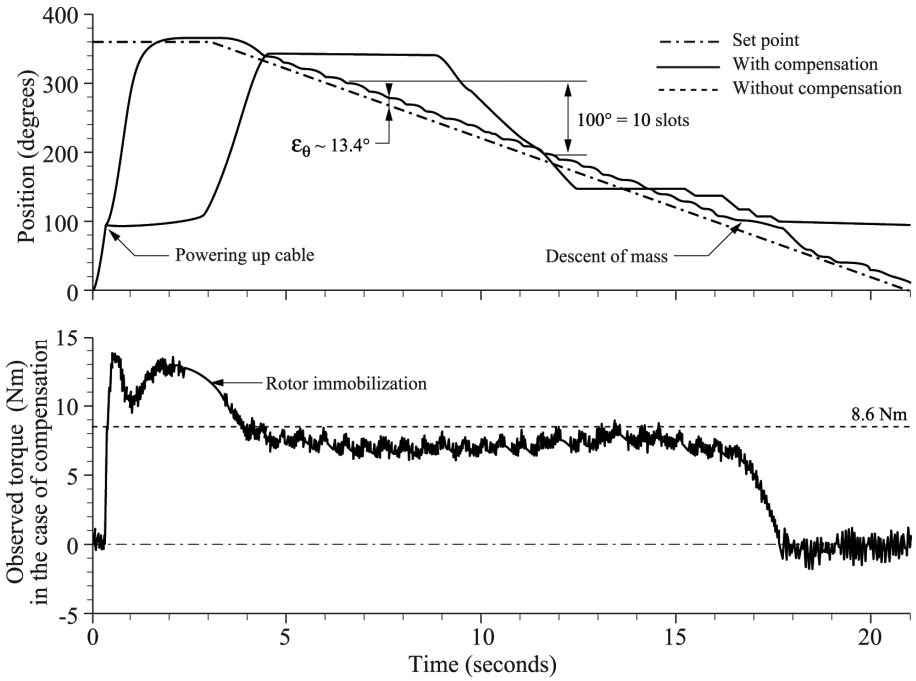

Figure 7.40. *Hoisting and descending of a 20-kg mass lifting*

During the set point step, torque peak, at power up, is caused by the mass acceleration torque, added to the torque created by the mass weight.

The observed torque decreases when the position is close to the set point, because the mass has a tendency to continue its momentum. Since the position does not reach the reference position, the set point and the observed torque increase to defeat friction and cogging torque. A small overshoot and decreasing of integral action occur. The latter acts on the set point and causes a decrease in the observed torque during the immobilization of the rotor.

In Figure 7.41, we note the fluctuations caused by the cogging torque, superimposed to the torque generated by the mass. They present a spatial period of 10°, according to the distribution of slots. The disruptions linked to the quantification of the measure of position also appear (Figure 7.41), based on the resolution of the encoder (approximately 0.7°). These two tests show the aptitude of the observer to compensate phenomena external and internal to the actuator. The load torque is external, independent from the actuator. But the cogging torque is a phenomenon strictly internal to the actuator. The observer is very efficient in "absorbing" torque effects (Figure 7.40).

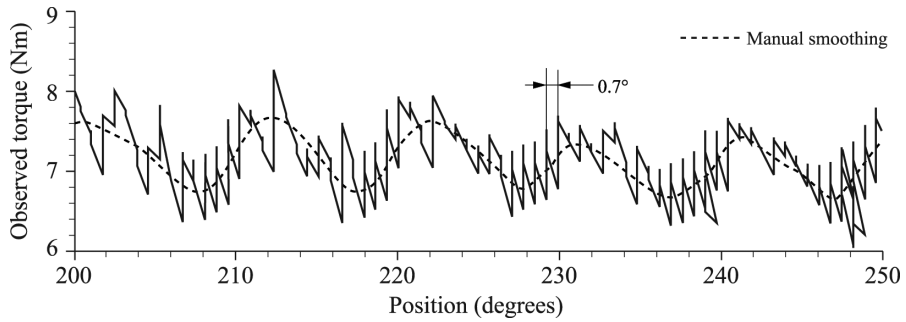

Figure 7.41. *Torque observed according to position*

7.6.2.2. *Variation of the friction factor*

The tests described in the following text illustrate the behavior of the actuator when it experiences friction factor variations. The modification of this factor is obtained by cabling the direct current machine to the brake generator with resistive load equaling 2.3 Ω; the excitation current of the direct current machine is equal to 0.45 A.

In these conditions, the friction factor is multiplied by a factor of 5. The state feedback and observer dynamics are characterized by:

$$\omega_{bf} = 5 \text{ rad/s}, p_{obs} = p_1 = p_2 = 0.65, 7 \Rightarrow \omega_{obs} \sim 86 \text{ rad/s} \quad \text{(double pole)}$$

The results, obtained with position set point steps of different amplitudes (1, 4, and 5 tours) are presented in Figure 7.42. They show the efficiency of the observer to ensure robustness of the actuator. When the disruption torque is compensated, the position has no overshoot, contrary to the case without compensation.

We can, however, observe a gap between observed torque and measured torque for the important steps of the set point. This gap can be due to the saturation of the synchronous machine.

For large-amplitude steps, current control reaches values equal to over four times the rated current. If the nominal operation is in the saturation elbow, saturation appears for the current values applied. Because of this saturation, the flux and torque are no longer proportional to currents. Saturation leads to a decrease in the machine's torque constant. The control algorithm, feeling the effects of this decrease on the output variables, increases the current set point consequently in order for the motor to provide the corresponding torque to the dynamic imposed.

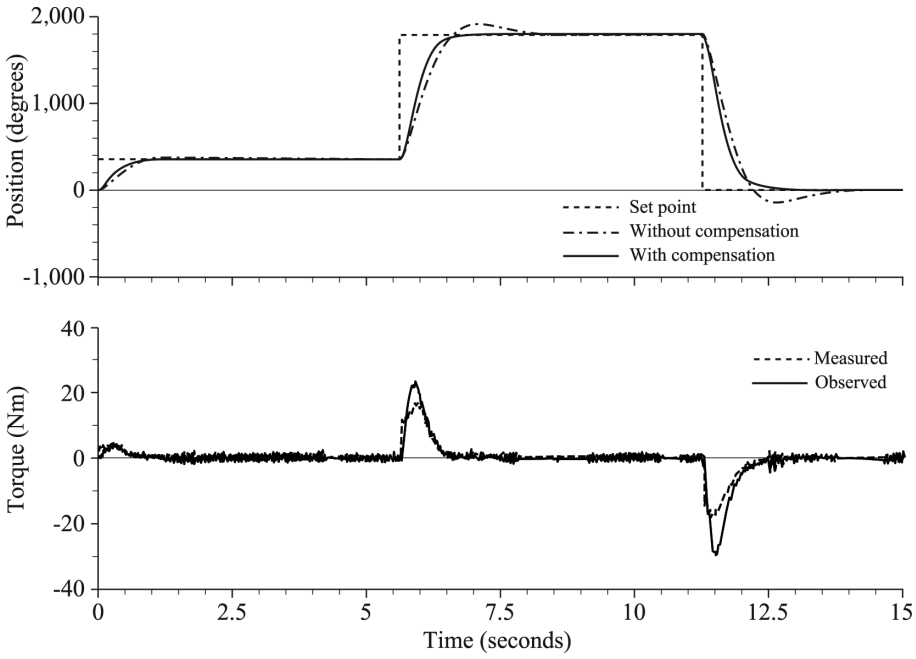

Figure 7.42. *Consideration of friction factor variation*

This increase of the current set point is taken into consideration by the observer; it provides a higher observed torque than the measured torque. The observer factors have not been modified and correspond to the nominal parameters of the synchronous machine.

This saturation problem does not exist on magnet machines where the flux is imposed and the equivalent air gap is important. In a transitory way, torque peaks can be very important.

In this way, the torque constant of the synchronous machine decreases because of the saturation of its magnetic circuit.

Another cause can be the deterioration of the behavior in current source of the inverter during excessive actuator speed, thus generating too large counter electromotive forces affecting the gain of the current source. In order to avoid this situation, the speed of the actuator was limited to 500 rev/min in these tests.

Since the angle position is reached, the torque experiences oscillations caused by the combined effects of position measure quantification and observation dynamic. These oscillations are especially present with zero load torque.

These tests show the ability of the observer to maintain actuator robustness during variations of friction factor and torque constant.

7.6.2.3. *Influence of the inertia variation*

As before, control law is state feedback with resistant torque observation. We compare the behavior of the actuator with or without load torque compensation. The dynamics for the state feedback and observer are characterized by:

$$\omega_{bf} = 5 \text{ rad/s}, p_{obs} = p_1 = p_2 = 0.75 \Rightarrow \omega_{obs} \sim 58 \text{ rad/s} \quad \text{(double pole)}$$

Simulation of inertia is obtained with the help of the four quadrant chopper (Figure 7.43), where current set point is proportional to the derivative of the measured speed, since the factor of proportionality is the inertia to simulate. This derivation must be done with care to avoid adding excessive noises in the current set point. A second-order digital low-pass filter in the measured speed lessens the noises before derivation. The tests are done with additional inertia (Figure 7.44) of 0.055 kg m^2 (J_{sup}), and total inertia represents 2.7 times the nominal inertia. J_{sup} is canceled in the interval: $t \in$ [8.25 s; 12.15 s].

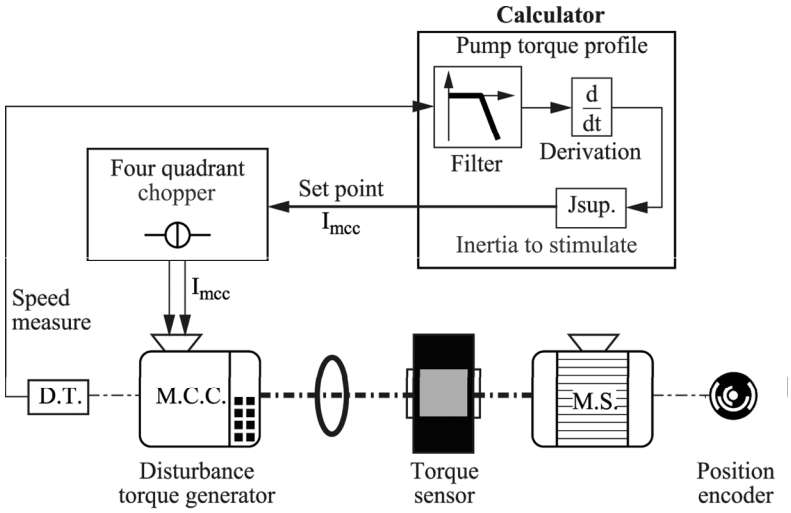

Figure 7.43. *Experimental simulation of additional inertia*

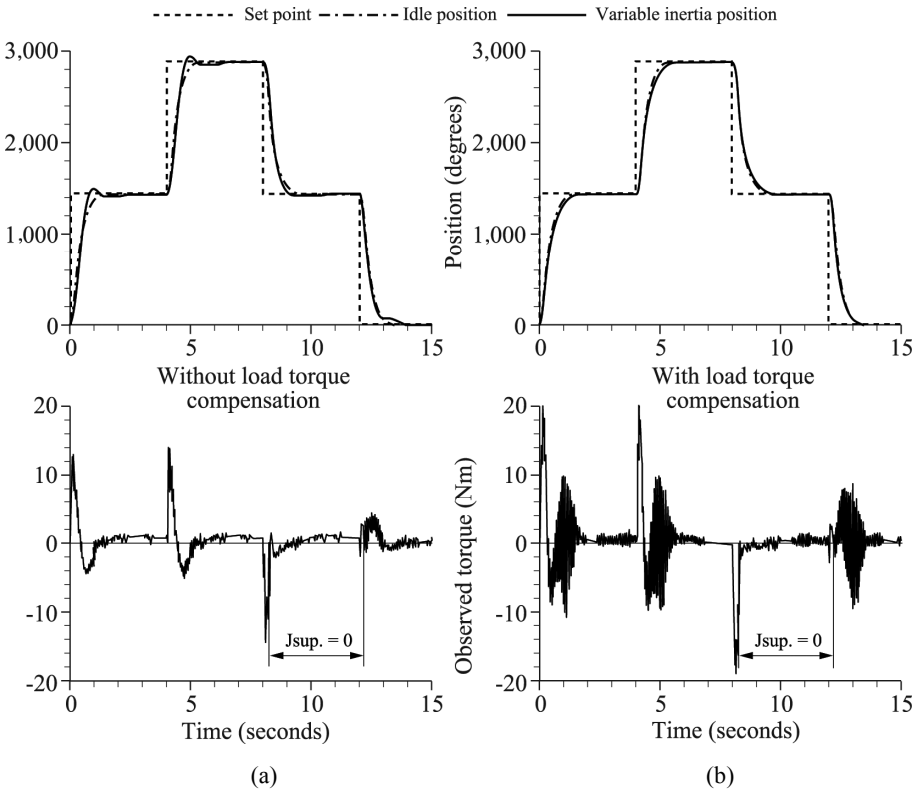

Figure 7.44. *Effects of a load torque inertia variation (a) without compensation and (b) with compensation*

In order to facilitate comparing tests, we present the position where the actuator works in nominal conditions (without additional inertia). The effect of load torque compensation clearly appears in the position reports. The overshoots (~50°) reduced, and the position report (Figure 7.44b) shows that the actuator with load torque compensation behaves almost in the same way, with no load, as with additional inertia. The abrupt variations of additional inertia are also well compensated.

During the cancelation of additional inertia (at 12.15 s), the position without compensation of load torque presents a small overshoot attributed to the excess of integration of the modal control reset action but does not exist when the torque is compensated. When the additional inertia is applied once more, the actuator without compensation shows abrupt slowdown, which is not the case with compensation.

The observed torque reports illustrate the effect of inertial load that is resisting in the phase of acceleration and driving in the braking phase. These effects are visible (Figure 7.44a) when additional inertia is applied.

The report (Figure 7.44b) presents the same characteristics in the first approximation, but the observed torque becomes oscillatory when the actuator reaches the set point position. These oscillations, due to the bandwidth limitations of the four-quadrant clipper, and the observer do not appear in simulation with perfect elements.

The observed torque is non-zero when the position no longer evolves. In this case, the torque should be zero, since the inertial torque is zero, when the angle steady state position is reached. This phenomenon is caused by static friction (see the next section).

7.6.3. *Non-linear friction influence*

In this section, the effects of non-linear friction on the actuator are studied. In the first part, a test highlights static friction at group steps level. It was done without compensating the load torque. In the second part, the same test is done by compensating the load torque.

7.6.3.1. *Static friction*

Static friction exists in group steps and is brought out in mass hoisting, which is then maintained in suspension. We then compare the observed and measured torques with the torque corresponding to the mass weight ($C_{pds} \sim 8.6$ Nm).

In this test, the load torque is not compensated and the observed speed is used for state feedback. The dynamics of the state feedback and observer are characterized by:

$$\omega_{bf} = 15 \text{ rad/s}, p_{obs} = p_1 = p_2 = 0.7 \Rightarrow \omega_{obs} \sim 71 \text{ rad/s (double pole)}$$

In Figure 7.45, static friction effects are emphasized. The observed and measured torques are not equal to the torque created by mass (C_{pds}) because the friction can be added to or deducted from C_{pds}. The static friction and dry friction torques are important for the radial forces at step level, located close to the pulley holding the mass.

Static friction is responsible for the gaps between real, measured, and observed torques when the actuator is stopped. By simulating C_{pds} with the direct current machine, the steps are not requested as much at the radial level and static friction is

insignificant. The existence of static friction is confirmed by an experiment where the conditions of adhesion internal to steps are modified when the position set point is reached. This modification is obtained by a mallet strike triggering a radial shock wave in the step most solicited by the hoisting forces, that of the direct current machine, closest to the hoisting pulley. The shock wave modifies the conditions of adhesion and reduces static friction, as the observed and measured torques converge with C_{pds}. The gap between measured torque and observed torque can be attributed to friction internal to the synchronous machine, not measured by torque sensor, placed after this friction. An analysis explains the gap signal between C_{pds} and measured torque.

It is based on the mechanical equation of the actuator:

$$J \cdot \underbrace{\frac{d\Omega}{dt}}_{\text{acceleration}} = C_{em} - C_{pds} - C_{frot} \qquad [7.91]$$

The term C_{frot} groups all the friction forces that can be considered, and the sign of this term is equal to the sign of speed.

In the following reasoning, the position reaches its set point without overshoot; this consideration is validated by the measure of error (Figure 7.45). The acceleration is positive in the final lifting phase ($t \sim 1.2$ s) so that the actuator is able to reach the position set point. The result then is:

$$C_{em} \geq C_{pds} + C_{frot} \qquad [7.92]$$

Since there is no overshoot, the speed is positive in the final hoisting phase. Friction torque C_{frot} is then positive at that moment. When the position leans toward its set point, the motor torque and speed decrease. Stiction occurs here causing the actuator to block, and blocking occurs before the motor torque is equal to the torque created by mass (C_{pds}). If this blocking occurs when the set point position is reached, the motor torque no longer evolves but is then greater than C_{pds}. The actuator must defeat dry and viscous friction in hoisting phase.

Because of blocking, speed and acceleration are zero and

$$C_{em} = C_{pds} + C_{frot} > C_{pds} \qquad [7.93]$$

The friction torque is different from zero because of static friction (at zero speed) confronting the motor torque excess in relation to C_{pds}. Static friction makes it possible to explain the motor torque excess influencing measured and observed torques.

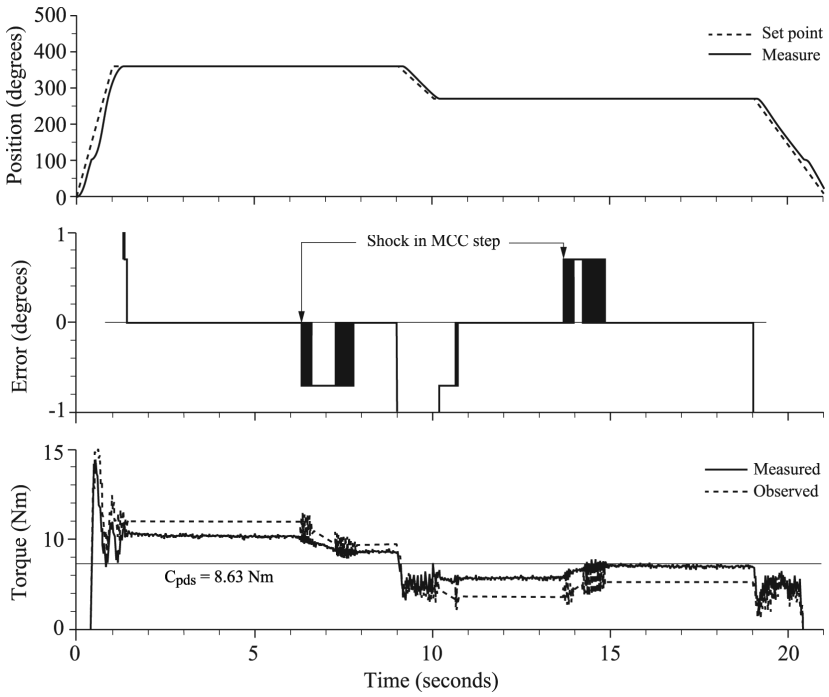

Figure 7.45. *Emphasis on static friction (experimental results)*

The shock wave modifies the conditions of adhesion, and consequently, reduces the maximum value of static friction. Relation [7.92] is once more verified, and the actuator moves as shown in error (Figure 7.45 at $t \sim 6.25$ s).

The error occurs in the low-weight encoder bit and is negative (overshoot), thus confirming the excessive value of the motor torque and triggering a decrease in control reset action. This decrease affects the motor torque, and the position comes back to its set point level. The observed and measured torques then converge to C_{pds}. In a symmetrical way, when the mass is partially down ($t > 9$ s), the C_{pds} underestimation is justified. Static friction then compensates a part of C_{pds} and the braking torque of the actuator is reduced.

7.6.3.2. *Influence of static friction on control law with resistant torque compensation*

We carry out mass hoisting by compensating the load torque. Then a limit cycle appears (Figure 7.46). This limit cycle is represented by a low-frequency angular backlash (0.6 Hz) on position. We show that the frequency of angular backlash and

the amplitude of observed torque variations depend on the hoisted mass. The heavier the mass, the more the frequency of angular backlash decreases and the more the amplitude of observed torque variations increases.

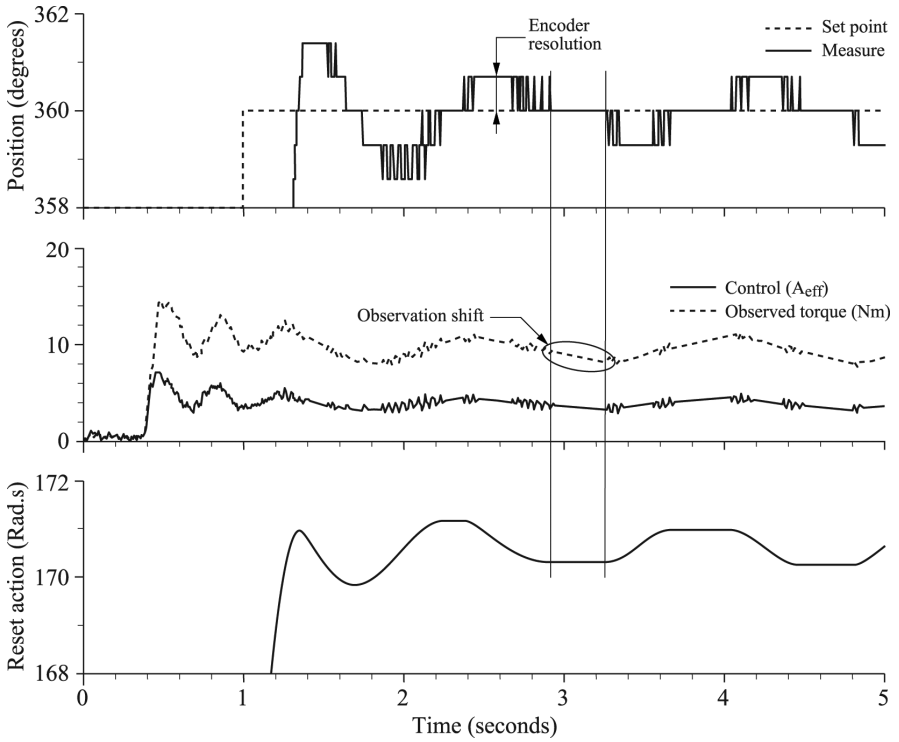

Figure 7.46. *Effect of non-linear friction, in the case of load torque compensation*

This angular backlash in the low-weight bit of the position encoder is linked to the observer. When the position is equal to the set point, the control variable changes, whereas the reset action, set point, position, and speed are constant. This control variation comes from the variation of the observed torque (Figure 7.46).

The variation of the control variable results from a drift of observation because of the non-linearity of friction. Static friction is at the basis of non-linearity. The observers previously studied are based on a linear actuator model; a variation of the control variable is affected without delay on the actuator output variables. Because of static friction, the actuator rotor, submitted to torque variations, remains blocked as long as these variations are lower than the maximum value of the static friction torque.

The observation structures use two variables, control and one of the actuator outputs (speed or position). With static friction, the control variable can vary without affecting the constant output variables. Variations of the observed variables are the images of those of control variables, as long as the actuator remains blocked. According to the study of observers, the observed torque changes as the control variable when the actuator is stopped. The control variable and observed torque (with blocked rotor) vary in the same way because of the load torque compensation. We are witnessing a drift by cumulative effect. It is a physical reality. When the sum of torques applied to the actuator rotor exceeds the maximum friction value, then the rotor leaves its attitude angle. The control law, by its reset action, brings the rotor back to its set point position.

The ability of the control law depends on the resolution of the position encoder to reduce the amplitude of the limit cycle (Figure 7.46).

Static friction makes the windage of observed torque possible when the actuator is immobile, at the origin of a low-frequency limit cycle [BRA].

In order to stop this limit cycle, we must get involved in the drift of torque observation. By blocking the observer recurrence in the equation, the observed torque remains constant. This torque is different from the external load torque because of static friction at step level but remains constant (Figure 7.47). The blocking of the recurrent equation is done with care so as not to distort torque observation. Observation drift, at the origin of the limit cycle, occurs when the error of position and speed are zero. Observation and recurrence in the case of the reduced order two observer are blocked [7.94]:

$$\varepsilon_\theta < 0.012 \text{ rd} \quad (\text{encoder resolution})$$

and

$$\Omega - \hat{\Omega} \leq 0.1 \text{ rd/s} \quad (\text{arbitrary choice})$$

7.7. Conclusion

The mechanical load drive, with the help of an electromechanical actuator, requires a rigorous control of electromagnetic torque. The quality of this control conditions the characteristics of the variable induction transmission all the more so that the load powered is complex in the sense of a certain uncertainty, and all the more so that rotation speed is low, or even zero. The work presented in this chapter proposes solutions for this problem, by implementing control structures based on the association of a powerful control law and a disturbance observer.

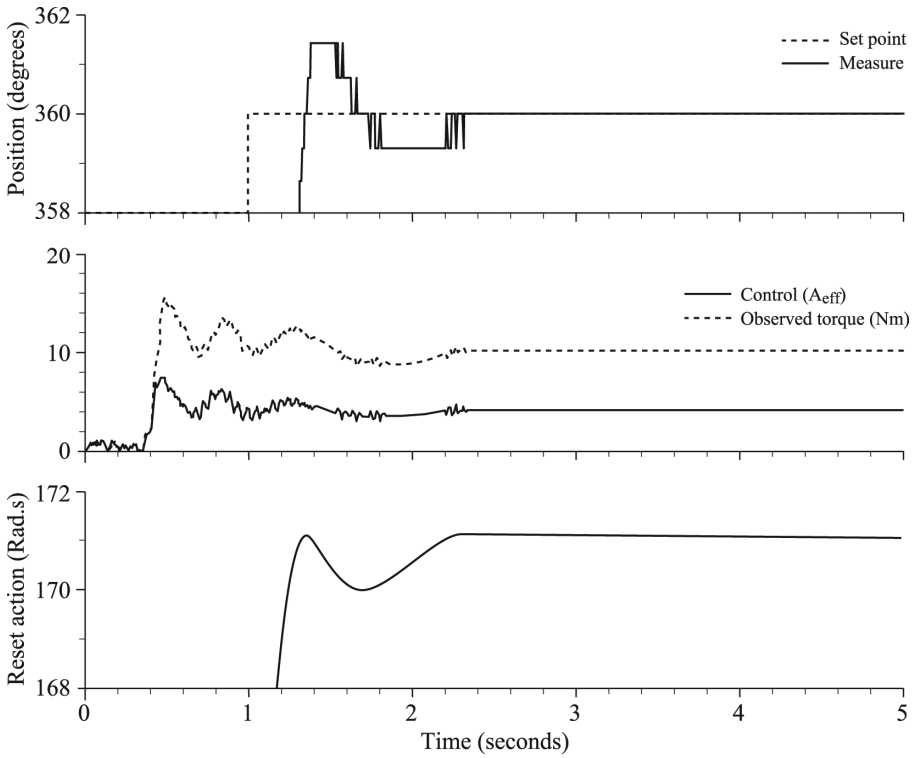

Figure 7.47. *Inhibition of the limit cycle (experimental results)*

The major contribution is linked to the design and development of a load torque observer to rebuild the disruptions affecting the axis of rotation. These disturbances can be internal to the actuator, as the cogging torque, the distortion of electromotive forces, or the modification of characteristics of friction between the moving part and the fixed part. But these disturbances can also be external or exogenous linked to useful torque impact or a specific characteristic of the load, for example, the presence of non-linear imbalance or clearance, or still a particular speed effort link. Nevertheless, the load observer imagined here must rebuild the efforts experienced by the axis in rotation independently from their nature and original causes. This quantity is then used in a correction loop to eliminate or at least reduce the effect of disruptions on measurable variables such as speed and/or position.

Different observers are studied here, different in terms of variables used in input and output, according to the volume of possible calculation (complete or reduced-order observer), and the dynamic imposed in relation to the parameter dynamic and sampling period. Sections 7.2.7 and 7.5.5 provide some elements for the choices

with respect to the candidate solutions that must be chosen according to parametric invariance and that measure quantification and the presence of measuring noises. In fact, the development elements become predominant on the structures proposed also involving the extent of parametric variations.

This last element also conditions sizing of control laws through nominal calculation parameters. Because of this, overestimating the friction factor and underestimating inertia play a beneficial role in the instability of the series.

In conclusion, we should note that at very slow speed, and even at the end, rigorous control of the axis is difficult because the information collection is altered, and it is necessary to settle for low evolutions ensuring observation and compensation. This is all the more difficult as the models of load representation are at the limit of their validity.

7.8. Bibliography

[BAB 91] BABARY J.P., *Représentation d'état des systèmes linéaires continus*, photocopy ENSEEIHT, Toulouse, 1991.

[BRA 87] BRANDENBURG G., SCHÄFER U., "Influence and partial compensation of backlash and Coulomb friction for a position-controlled elastic two-mass system", *Proceeding EPE*, Grenoble, 1987, p. 1041-1047.

[BÜH 82] BÜHLER H., "Réglages échantillonnés", *Presses Polytechniques Romandes*, vol. 1, Lausanne, 1982.

[BÜH 83] BÜHLER H., "Réglages échantillonnés", *Presses Polytechniques Romandes*, vol. 2, Lausanne, 1983.

[BÜH 88] BÜHLER H., "Correction de la composante intégrale de régulateurs analogiques et digitaux en cas de limitation", *SGA Zeitschrift—bulletin ASSPA*, p. 14-19, 1988.

[CER 95] CERRUTO E., CONSOLI A., RACITI A., TESTA A., "A robust adaptive controller for PM motor drives in robotic applications", *IEEE Transactions on Power Electronics*, vol. 10 no. 2, 1995, p. 62-71.

[CLE 95] CLENET S., VINASSA J.M., LEFEVRE Y., LAJOIE-MAZENC M., "Influence of the brushless dc motor torque compensation by acting on the current waveshapes on torque speed characteristics", *Proceeding EPE'95*, vol. 3, Seville, Spain, September 19-21, 1995, p. 898-902.

[COU 97] COURAULT J., "Applications industrielles de CEGELEC. Commande des machines à courant alternatif", Responsables scientifiques: Canudas De Wit C., Roye D., *Ecole d'été d'automatique de Grenoble*, session 17, September 8-12, 1997.

[FOC 89] FOCH H., "Electronique de puissance – Principes fondamentaux – Dualité dans les convertisseurs statiques", *Techniques de l'ingénieur*, article D 3154 vol. D3I, September 1989.

[FÖR 95] FÖRSTNER D., *Modélisation de la charge mécanique pour un variateur asynchrone, Rapport de stage dans le cadre d'échange ERASMUS* (TU Hamburg-Harburg), INP de Toulouse, LEEI, September 1995.

[GAN 66] GANTMACHER F.R., *Théorie des matrices. Tome 1, théorie générale*, Collection universitaire de mathématiques, Dunod, Paris, 1966.

[GAS 04] GASC L., Conception d'un actionneur à aimants permanents à faibles ondulations de couple pour assistance de direction automobile, approches par la structure et par la commande, INP, Toulouse doctoral thesis, 2004.

[GOM 92] GOMES S.C.P., Précision de la transmission du couple par un moto-réducteur électrique: modélisation et commande d'un bras rigide ou flexible avec compensation du frottement, Ecole Nationale Supérieure de l'Aéronautique et de l'Espace thesis, no. 102, 1992.

[HEC 86] HECTOR J., "DSN, un logiciel de manipulation de courbes", *Manuel de référence*, vol. 3.1, INP–ENSEEIHT, Toulouse.

[HOR 94] HORI Y., ISEKI H., SUGIURA K., "Basic consideration of vibration suppression and disturbance rejection control of multi-inertia system using SFLAC", *IEEE Transactions on Industry Applications*, vol. 30, no. 4, 1994, p. 889-896.

[IWA 93] IWASAKI M., MATSUI N., "Robust speed control of IM with torque feedforward control", *IEEE Transactions on Industrial Electronics*, vol. 40 no. 6, 1993, p. 553-560.

[JOH 92] JOHNSON C.T., LORENZ R.D., "Experimental identification of friction and its compensation in precise, position controlled mechanisms", *IEEE Transactions on Industry Applications*, vol. 28 no. 6, 1992, p. 1392-1398.

[KAB 96] KABBAJ H., VORWALD P., FADEL M., "Adaptive position control of a synchronous drive fed by a ZVSPWM inverter, using on line identification and self-tuned RST controller", *Proceedings ELECTRIMACS'96*, September 17-19 Saint-Nazaire, 1996, p. 929-933.

[KO 93] KO J.S., LEE J.H., CHUNG S.K., "A robust digital control of brushless DC motor with dead beat load torque observer", *IEEE Transactions on Industrial Electronics*, vol. 40, no. 5, 1993, p. 512-520.

[LAJ 91] LAJOIE-MAZENC M., VIAROUGE P., "Alimentation des machines synchrones", Techniques de l'ingénieur, vol. D3II, article D 3630, 1991.

[LAN 88] LANDAU I.D., *Identification et commande des systèmes*, Hermes, Paris, 1988.

[LAN 86] LANDAU I.D., DUGARD L., *Commande adaptative – Aspects pratiques et théoriques*, Masson, Paris, 1986.

[LEP 93] LE PIOUFLE B., "Comparison of speed non-linear control strategies for the synchronous servomotor", *Electric Machines and Power Systems*, vol. 21, no. 2, 1993, p. 151-169.

[LIG 95] LIGIER J.L., "Matériaux pour paliers lisses", *Techniques de l'ingénieur*, vol. B5II, article B5330, 1995.

[LOC 97] LOCHOT C., ROBOAM X., DE FORNEL B., MOLL F., "High speed railway traction system modeling for simulating electromechanical interactions", *Proceeding of World congress on railway research*, Florence, Italy, November 1997.

[LON 95] LONGCHAMP R., *Commande numérique de systèmes dynamiques*, Presses Polytechniques et Universitaires Romandes, Lausanne, 1995.

[LUE] LUENBERGER D.G., "An introduction to observers", *IEEE Transactions on Automatic Control*, vol. AC-16, 1971, p. 596-603.

[MAR 65] MARCUS J., *Echantillonnage et quantification*, Gauthier-Villars, Paris, 1965.

[MAX 88] MAX J., "Pratique du filtrage – Filtrage numérique", *Techniques de l'ingénieur*, vol. R3, article R 1105, 1988.

[MET 92] METZ M., ROUX J., BEN DOUA S., ARCHES J.P., FOCH H., "New ZVS-PWM inverter switching limits and operating area", *IEEE Proceedings B*, vol. 139, no. 2, 1992, p. 86-95.

[MOU 97] MOULINIER P., "Editorial – Le navire tout électrique", *Revue de l'Electricité et de l'Electronique*, no. 3, 1997, p. 1.

[MTH 91] WOLFRAM S., *Mathematica, A System for Doing Mathematics by Computer,* 2nd ed., Addison-Wesley, Redwood City, California, 1991.

[MTS 93] MATSUI N., MAKINO T., SATOH H., "Autocompensation of torque ripple of direct drive motor by torque observer", *IEEE Transactions on Industry Applications*, vol. 29, no. 1, 1993, p. 187-194.

[MUR 93] MURAKAMI T., YU F., OHNISHI K., "Torque sensorless control in multidegree-of-freedom manipulator", *IEEE Transactions on Industrial Electronics*, vol. 40, no. 2, 1993, p. 259-265.

[OHN 94] OHNISHI K., MATSUI N., HORI Y., "Estimation, identification, and sensorless control in motion control system", *Proceedings of the IEEE*, vol. 82, no. 8, 1994, p. 1253-1265.

[REI 91] REIS COSTA J.C., FADEL M., DE FORNEL B., "Commande numérique d'axe avec compensation du couple résistant", *Journal de physique III*, vol. 1, no. 3, March 1991, p. 465-479.

[RIO 96] RIOS QUESADA J., *Loi de commande pour le positionnement et observateur de force électromotrice d'un ensemble convertisseur-machine synchrone*, Rapport de DEA en "Génie Electrique", UPS-INP, Toulouse, 1997.

[ROT 95] ROTELLA F., *Théorie et pratique du calcul matriciel*, Technip, Paris, 1995.

[SEV 82] SEVELY Y., JOUVE P., "Le calculateur numérique dans la conduite des procédés", *Techniques de l'ingénieur*, vol. R7, article R 7110, 1982.

[THI 96] THIESEN H., Onduleur MLI à commutation douce—Application à la génération électrique—Etude et réalisation de la commande, Institut National Polytechnique de Toulouse thesis, no. 1140, 1996.

[THO 97] THOMAS J.L., POULLAIN S., "Commande des machines à courant alternatif: point de vue de la recherche industrielle", Commande des machines à courant alternatif. Scientifiques responsables: Canudas De Wit C., Roye D*., Ecole d'été d'automatique de Grenoble*, session 17, September 8-12, 1997.

[VER 88] VERGHESE G.C., SANDERS S.R., "Observers for flux estimation in induction machines", *IEEE Transactions on Industrial Electronics*, vol. 35, no. 1, 1988, p. 85-94.

[VIB 95] VIBRO-METER*, Notice d'utilisation – Torquemaster de la série TM 200 - P/N 648*. 012 F. Edition 4. Fribourg, Switzerland, July 1995.

[VOR 92] VORWALD P., Contrôle en position de la machine synchrone autopilotée entraînant une charge variable. *Rapport de DEA en "Génie Electrique"*, UPS-INP, Toulouse, 1992.

[VOR 95] VORWALD P., KABBAJ H., FADEL M., DE FORNEL B., "Position control of a synchronous drive fed by a ZVSPWM inverter, using state control and load torque observation", *Proceeding PES Stockholm Power Tech – Electrical machines and drives, IEEE-PES/KTH*, June 18-22, 1995, p. 29-34.

[VOR 96] VORWALD P., "Contrôle en position de la machine synchrone basé sur une structure optimale de réglage d'état associée à un observateur de couple résistant", *Firelec – 3e conférence des jeunes chercheurs en* "*Génie électrique*", Lyon, April 1996, p. 142-145.

[WES 94] WESTERHOLT E.G.V., *Commande non linéaire d'une machine asynchrone – Filtrage étendu du vecteur d'état – Contrôle de la vitesse sans capteur mécanique*, Institut National Polytechnique de Toulouse, no. 851, 1994.